La borsa di dottorato è stata cofinanziata con risorse del
Programma Operativo Nazionale Ricerca e Innovazione 2014-2020 (CCI 2014IT16M2OP005),
Fondo Sociale Europeo, Azione I.1 "Dottorati Innovativi con caratterizzazione Industriale"

UNIVERSITÀ DEGLI STUDI DI SALERNO

Dipartimento di Ingegneria Civile

Dottorato di Ricerca
in
Rischio e Sostenibilità nei sistemi dell'Ingegneria civile, edile e ambientale"
Curriculum in *Ingegneria delle strutture e del recupero edilizio ed urbano*

XXXII Ciclo (a.a. 2018-2019)
Tesi di dottorato in Scienza delle Costruzioni

MODELING AND DEVELOPMENT OF INNOVATIVE STRUCTURES FOR SMART FAÇADES OF ENERGY EFFICIENT BUILDINGS

Raffaele Miranda

Il Tutor
Prof. Fernando Fraternali

Il Coordinatore
Prof. Fernando Fraternali

MODELING AND DEVELOPMENT OF INNOVATIVE STRUCTURES FOR SMART FAÇADES OF ENERGY EFFICIENT BUILDINGS

Abstract

Recent studies have proposed the use of tensegrity structures in the field of Energy Efficient Buildings for the construction of dynamic shading systems of new generation intelligent buildings, thanks to the special ability of such structures to act as systems for deployment and to provide minimal mass structures for a variety of loading conditions.

This dissertation presents a mechanical study on the use of tensegrity lattices for the design of energy efficient sun screens. Tensegrity systems are lattice structures whose compression elements (or bars) can be described as rigid partially deformable bodies, while cables (or strings) are tensile elements and are usually pre-stretched to stabilize compressed members.

Inspired by the dynamic solar façades of the Al Bahar Towers in Abu Dhabi we studied a tensegrity solution for the solar screen module and simulated the mechanical analysis with the related numerical results. The analyzed screens origami modules formed by the repetition of a basic tensegrity system that constitutes an eye of the façade. The actuation of each module is controlled through the stretching of the perimeter strings, which form macro-triangles moving parallel to the building, while all the bars and the fabric mesh infills form micro-triangles that are allowed to move rigidly in space. We developed an analytic formulation of the deformation mapping associated with such an actuation motion, giving rise to a morphing-type behavior. We also estimated the energy required to activate the analyzed shading system, and established a comparison between its weight and that of the original screens of the Al Bahar Towers.

The basic module of the examined screens includes tensegrity units with displacement amplification properties that are equipped with piezoelectric cables. A numerical procedure for the simulation of the dynamic response of the examined sunscreens under arbitrary loading is formulated. The proposed model is employed

to study the actuation motion exhibited by the elementary origami module, and its vibrations under the action of wind forces. The peculiar ability of tensegrity shading systems to harvest the mechanical energy stored in the strings is investigated, by drawing comparison with the energy harvesting abilities of photovoltaic panels and microeolic turbines. The proposed tensegrity design concept leads to the realization of shading screens that are markedly lightweight, operate on very low energy consumption and can be usefully employed to harvest solar and wind energies.

Pubblications

The work presented in this dissertation originated the following articles published in international scientific journals:

- **R. Miranda**, E. Babilio, N. Singh, F. Santos, F. Fraternali, Mechanics of smart origami sunscreens with mechanical energy harvesting ability, MECHANICS RESEARCH COMMUNICATIONS, 2020, 103503, ISSN: 0093-6413, DOI: 10.1016/j.mechrescom.2020.103503;

- E. Babilio, **R. Miranda**, F. Fraternali, On the kinematics and actuation of dynamic sunscreens with tensegrity architecture. FRONTIERS IN MATERIALS (MECHANICS OF MATERIALS), 2019, 6:7. ISSN: 2296-8016, DOI: 10.3389/fmats.2019.00007;

- Cimmino, M.C., **Miranda, R.**, Sicignano, E., Ferreira, A. J. M.; Skelton, R. E., Fraternali, F. Composite solar façades and wind generators with tensegrity architecture. COMPOSITE. PART B, ENGINEERING, ISSN: 1359-8368, Online first (2016), DOI: 10.1016/j.compositesb.2016.09.077;

During the course of my PhD studies, I have also acted as co-author of the following indexed conference proceedings:

- **R. Miranda**, E. Babilio, G. Carpentieri, F. Fraternali. Composite sunscreens with tensegrity architecture. 22nd International Conference on Composite Structures (ICCS22) and 1st Chinese Conference on Composite Structures (CCCS1), 22-25 October 2019, Wuhan, China;

- E. Babilio, **R. Miranda**, G. Carpentieri, F. Fraternali. Active tensegrity shells of energy efficient buildings. XXIV Conference- Italian Association of Theoretical and Applied Mechanics (AIMETA), 15-19 September 2019, Rome, Italy;

- **R. Miranda**, E. Babilio, A. Amendola, I. Mascolo, F. Fraternali, Design and control of adaptive tensegrity sunscreens. 7th International Conference on Structural Engineering, Mechanics and Computation (SEMC), 2-4 September 2019, Cape Town, South Africa;

- A. Amendola, I. Mascolo, **R. Miranda**, F. Fraternali. Optimal prestress design of the bandgap dynamics in tensegrity metamaterials. 7th International Conference on Structural Engineering, Mechanics and Computation (SEMC), 2-4 September 2019, Cape Town, South Africa;

- E. Babilio, **R. Miranda**, G. Carpentieri, F. Fraternali. Computational modelling of the dynamics of active sunscreens with tensegrity architectures. Computational Methods in Structural Dynamics and Earthquake Engineering (COMPDYN 2019), 24-26 June 2019, Crete, Greece;

- A. O. Krushynska, A. Amendola, **R. Miranda**, C. Daraio and F. Fraternali. Harnessing tensegrity to design tunable metamaterials for broadband low-frequency wave attenuation. Computational Methods in Structural Dynamics and Earthquake Engineering (COMPDYN 2019), 24-26 June 2019, Crete, Greece;

- Babilio, **R. Miranda**, G. Carpentieri, F. Fraternali. On the dynamics of tensegrity sunscreens. ICoNSoM 2019. International Conference on Nonlinear Solid Mechanics, 16-19 June 2019, Roma, Italy;

- **R. Miranda**, A. Amendola, F. Fraternali. Use of tensegrity lattices for the actuation of origami sunscreens. 2019 International Workshop "Multiscale Innovative Materials and Structures" (MIMS2019), Cetara (SA), Italy, February 28th – March 2nd, 2019;

- A. Orefice, **R. Miranda**, G. Mancusi. 2-D lattice structures and band gaps. A numerical analysis. 10th European Solid Mechanics Conference (ESCM2018), 2-6 July 2018, Bologna, Italy;

- **R. Miranda**, F. Fabbrocino, M. Matheou, M.C. Phocas, F. Fraternali, Adaptive tensegrity structures for dynamic facades of energy efficient buildings, AIMETA 2017 - Proceedings of the 23rd Conference of the Italian Association of Theoretical and Applied Mechanics, Salerno, Italy, September 4-7 2017, vol. 1, pp.1074-1081, ISBN: 978-889-42484-7-0 (E-Book of Proceedings available at www.aimeta2017.unisa.it/node/53). Scopus:2-s2.0-85045560985;

- **R. Miranda**, M. Titirla, L. Feo, F. Fraternali. Use of composite lattice structures for kinetic envelops of energy efficient buildings. ICCE-25 – the

25th Annual International Conference on Composites and Nano Engineering, July 2017, Rome, Italy;

- **R. Miranda**, F. Fabbrocino, E. Sicignano, R. E. Skelton, F. Fraternali. Innovative structures for dynamic solar façades. 6th International Conference on Computational Methods in Structural Dynamics and Earthquake Engineering (COMPDYN 2017). June 2017, Rhodes Island, Greece;

- Cimmino, M.C., **Miranda, R.**, Sicignano, E., Ferreira, A. J. M.; Skelton, R. E., Fraternali, F. Solar façades with tensegrity architecture, 2016 International Workshop "Multiscale Innovative Materials and Structures" (MIMS2016), Cetara (SA), Italy, Oct. 28-30, 2016 (E-Book of Proceedings), DOI: 10.13140/RG.2.2.21778.86728.

To my family

Acknowledgments

A noticeable part of the present thesis work has been carried out during visits at the following research groups and companies, which are greatly acknowledged for their generous assistance and valuable support:

***Department of Structural Engineering and Caltrans Testing Facility*, University of California, San Diego, USA**.
Collaboration with Gianmario Benzoni's research group on the mechanical modeling of tensegrity systems.

***"PANDORA GROUP Srl"* (Napoli).**
Collaboration with the architect Alessia Guarnaccia on the architectural and technological aspects of tensegrity structures in relation to the modeling of hybrid façade systems.

The author also wishes to thank:

Fernando Fraternali, Enrico Babilio, Felipe Santos, Gerardo Carpentieri, Ada Amendola, Giuseppe Rocchetta, Mariella De Piano, Narinder Singh, Ida Mascolo, Diana Pena, Arnas Majumder.

for their precious advices, collaboration, essential support and solidarity during the course of the present work.

Thanks you all, ***Grazie a tutti***

Contents

LIST OF FIGURES

LIST OF TABLES

Part I. Introduction

Sustainable architecture is aimed to design and build buildings to limit environmental impact, mainly focusing on the energy efficiency, improvement of health, comfort and indoor air quality, reachable through measures and appropriate construction techniques. To design sustainable buildings means considering the fundamental elements of the design process, that are natural ventilation systems, orientation and shading, but also the adoption of new advanced technologies such as home automation systems or systems exploitation and management of renewable energy. The European Union requires Member States to develop long-term national plans to encourage efficient redevelopment of buildings to reduce emissions by between 80% and 95% compared to 1990. Furthermore, they are obliged to identify a long-term strategy that facilitates the transformation of residential and non-residential buildings into efficient and decarbonized structures by 2050, with the aim of achieving almost zero energy [1]. Nowadays, both in Italy and in Europe as a whole, a significant number of residential and industrial buildings have exceeded, in the absence of targeted interventions, the performance efficiency limit, thus making it necessary to plan interventions to recover the existing quality/energy deficit.

Among the objectives of the EU's Horizon 2020 program on the "Secure, Clean and Efficient Energy" (SC3) social challenge is the reduction of the energy consumption and the carbon emissions through an intelligent and sustainable employment of these resources, in order to pursue a more ambitious energy policy and to maintain current living standards while reducing energy dependence on fossil fuels. The demand for energy savings and the excessive CO_2 emissions generated by buildings has called for the use of new "interactive building envelopes", defined as systems that interacts with the variations of the external climatic conditions by means of automatic control devices, optimizing the environmental performance of the internal microclimate.

Sustainable engineering and architecture aim at designing buildings with limited environmental impact and high energy efficiency, comfort and indoor air quality, through appropriate construction techniques [2]-[4]. A sustainable design approach looks at the optimal design and control of natural ventilation systems, building orientation and shading, through passive and/or active techniques. The latter calls for the incorporation of home automation systems and renewable energy supplies within the building, typically in correspondence with the buildings "skin" [5],[6].

Human beings have developed increasingly complex envelope systems and components capable of ensuring good living conditions for each room, with the aim to create artificial places in which to conduct the primary activities of living. Over time architectural elements have therefore evolved from simple shelters from the elements (rain, wind, sun, intrusion of people or animals, cold, hot, etc.) to representative elements of the society (thanks to formal and material solutions), to an indoor comfort control system (through quantity and quality of light, ventilation, heating and cooling).

1.1 Energy Efficient Buildings

High energy efficiency building means "a construction capable of ensuring a well-being condition within it by minimizing the use of non-renewable energy sources" [8] in which indoor air quality and the achievement of thermo-hygrometric comfort are not delegated exclusively to technical components of "active" type, but are obtained through architectural typological solutions of "passive" or hybrid type.

The 2010 Energy Performance of Buildings Directive (EPBD) [9] made nearly zero-energy buildings (nZEB) the required norm for the design of new buildings in the EU from 2021, while for the public authorities, this requirement came into force from 2019. This directive gives Member States the responsibility to establish the minimum requirements for the energy performance of buildings and construction elements. Nowadays, buildings account for approximately 40% of final energy consumption in the European Union (Fig. 1), value remained more or less unchanged from 2014 to 2019. The EU Challenge is rooted in the need to maintain current living standards while reducing energy dependency on fossil fuels and pursuing a more ambitious environmental-climate policy.

After the Kyoto agreements on climate change, born as a result of developments in international environmental policy, the International Energy Agency has developed a series of scenarios and forecasts on energy development internationally for 2030 and 2050. This study shows how the sector of construction remains after the industry sector in which the greatest consumption of energy will be recorded in the face of a constant emission of CO_2.

Despite the partial failure of the agreements regarding the reduction of greenhouse gas emissions, many countries have launched policies that promote energy efficiency

in several sectors with the aim of reducing greenhouse gas emissions and limiting energy dependence on fossil fuels.

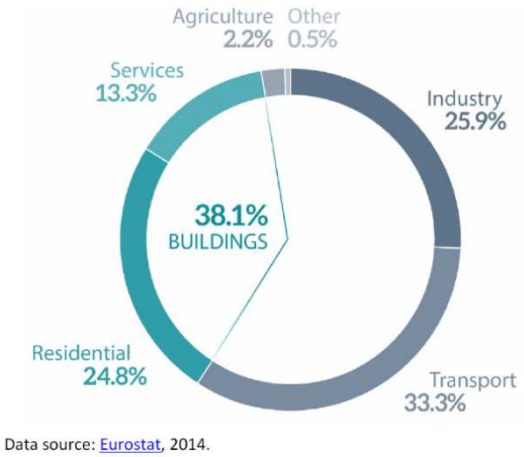

Figure 1.1: Energy consumption by sector in the EU-28 (reproduced with permission from https://epthinktank.eu/).

The energy technologies on which a new green economy is aimed are mainly those related to the renewable energy and energy efficiency sector. The latter, at the international level, plays a fundamental role, both for the variety of technologies that pertain to it and for its implications in the productive and commercial field. In fact, energy efficiency is related to different productive sectors: from residential to industrial, passing through the tertiary and transport sectors.

The importance that is attributed to the field of energy efficiency derives from the reduction of carbon dioxide emissions, the improvement of energy security and the containment of fossil demand. In the residential and tertiary sector, the main energy consumption is intended for air conditioning (winter and/or summer), and consequently for the production of domestic hot water, electricity and gas. Therefore, sustainable development is closely linked to the need to propose new forms of energetically aware living that guarantee adequate conditions of comfort to the users and limiting the environmental impact.

Among the main energy interventions to be promoted we recall the development and industrialization of technologies that allow energy conservation and the integration of active solar systems for new or existing buildings. In fact, the need to develop solar shading systems capable of ensuring flexible and adequate energy performance in the most severe climatic conditions, has led to investigate the issue of solar

shading trying to develop a new façade component characterized by the possibility of varying its configuration in the arc of the day according to the intensity of the sun's rays.

Nowadays there is a growing interest toward the design of double skin envelope systems of Energy Efficient Buildings (EEBs), which are able to influence the bioclimatic performance of the building (double-shell systems). Their main function is based on the ability to bring benefits to internal environments, in particular by acting through thermal and acoustic insulation, natural ventilation and the control and directionality of solar radiation (shading systems), and the ability to balance energy exchanges between the outside and inside. Therefore, the envelope plays a decisive role in the design of new generation buildings as it is configured as a dynamic system of environmental filters that can be used for the "metabolism" of buildings.

1.1.1 The building envelope

According to Horizon 2020, European Commission Programme for Research and Innovation, one of the most important components to be addressed within an innovative approach to Energy Efficient Buildings is the building envelope [10]-[12]. The building envelope must meet more functions than just the separation of the outer space from the interior with insulation, minimizing the energy consumption due to air conditioning. Energy efficiency can be mainly achieved reducing energy demand, making economical use of non-renewable energy sources and through the reduction of carbon dioxide emission.

The technological performance to be guaranteed for the building envelope in order to increase energy efficiency in the summer months can be sought in controlling the incident solar radiation through dynamic solar shading systems. Nowadays, the challenge of designers, in the field of smart façade systems, is to design a façade that can dynamically manage climate variability, in an optimally oriented way, to control internal thermal conditions and to improve the psychophysical well-being of the users.

The envelope has moved from being an energetically passive to a dynamic and interactive element of the complex energy system that regulates building operation. The gradual freeing of the outer skin from a structural function has had the inevitable consequence of a split between envelope and structure. The envelope is released from the load-bearing structure and becomes a closure element used mainly to adjust energy flows linked to the passage of heat, light transmission for adequate

illumination of the interior and the protection of the solar radiation in the months with higher temperatures.

An overview of the constructive scene shows that new types of double skin smart envelope must be able to form any kind of shape, even the most complex, as well as protecting the external surfaces of the building from sunshine.

The demand for high energy efficiency buildings inevitably leads to the emergence of design and technological solutions able to minimize the consumption of electrical energy deriving from the air conditioning systems, as well as to store wind and solar energy through integrated photovoltaic systems and / or solar panels for hot water and wind energy storage systems. Nowadays, the technologies and design skills to design and build "almost zero" energy buildings are many and can be listed in the following:

- The principles of sustainable and bioclimatic design must be followed with an integrated approach between the architectural and engineering component.
- The building must be compact and oriented so as to optimize the influence of the Sun.
- The casing (walls, floors and fixtures) must be very isolated and shaded to avoid heat dispersion and overheating respectively.
- The systems must operate at low temperatures (condensing boilers and heat pumps).
- Renewable energy production plants (photovoltaic and solar thermal) must be installed.
- Energy consumption must be constantly monitored.

The overall objective of the European Union strategy is to progress towards the decarbonisation of the EU economy by 2030 and beyond, while strengthening economic growth, consumer protection, innovation and competitiveness.

A simple darkening system does not always provide the necessary darkening of the interior spaces of a building: the different orientations of the façades, the daily and annual trend of the sun would require façades that, hour after hour, change configuration guaranteeing internal thermal hygrometric well-being.

The dynamic façade system is an innovative solution able to improve the energy saving of the building by responding precisely to external climatic variations and guaranteeing an optimal internal microclimate [13] - [16]. Dynamic façades are able

to quickly adapt to external conditions and offer a solution to generate low-impact buildings by eliminating the installation of air conditioning systems.

Referring to the standards established by European and Italian laws and according to the tensegrity operating principles, in this work innovative intelligent façade systems are developed, in order to evaluate the potential effects of the application of this envelope technology. These external architectural solutions would increase the value of buildings in terms of functionality, aesthetics and innovative energy design [17] - [20].

The success or failure of energy policies in the next deaths will be entrusted to interventions in the building sector. The pivotal element in the field of construction appears to be the building envelope, which has the role of regulating energy flows between the internal and external environment.

The term envelope was introduced in the building sector quite recently and means "everything that externally wraps something", thus defining a complex system that often becomes a structural element readable in section. This space of transition, the threshold between inside and outside, is completely independent of the content of the building. It is therefore possible to define the envelope as a system of integral closure of the building: system as it consists of several strictly interdependent technical elements, and full closure thanks to the continuity of the elements that compose it. The architectural envelope has evolved from a mainly barrier element into a complex, selective and multi-purpose filter system. The evolution took place in the sense of the transformation of massive and heavy structures into lighter and thinner systems designed to emancipate the functions of the building from those of the building.

The attention of contemporary research must be directed precisely towards the concept of envelope as a frontier, a permeable and selective dynamic interface, through which the process of interaction between the internal environmental elements and the external world can be realized, able to allow wellbeing and comfort in the inhabited spaces. The malfunctioning of modern buildings can be attributed to the fact of having designed the envelope in a completely formalistic way, paying little or no attention to exogenous climatic conditions. The task of maintaining the required internal conditions is entrusted to air conditioning systems, with inevitable waste, inefficiencies and poor functioning. Nowadays, the new criteria of energetic sustainability suggest to formulate a new approach to design that cannot be based only on aesthetic-formal research but must propose solutions adaptable to different environmental contexts.

In building automation, the building envelope is dynamically understood, as a system that interacts in an articulated and efficient way with the environment and all the buildings in the building, ensuring comfort inside and minimizing energy consumption.

The integrated management of the building envelope and the entire building is sought through the interaction of its subsystems such as:

- ventilation of double-skin facades;

- the external and internal shadow;

- lighting;

- HVAC central units (heating and air conditioning);

- integration with photovoltaic power plants.

To achieve this result a multisectoral approach is needed, exploiting both active and passive technological systems, considering the introduction of integrated technology in the building, such as the construction of an integrated photovoltaic system or natural ventilated façades.

1.1.2 Scope and aims

A great challenge that contemporary sustainable architecture has to face is to optimize natural resources and minimize energy consumption. Such a goal calls for the design of flexible and adaptive building envelopes able to react dynamically based on the evolution of the external climatic and environmental conditions.

This work is focused on the study initiated in the design of tensegrity shading systems with the aim of mitigating air conditioning consumption and optimizing energy performance of the buildings. It concerns the design of active solar façade screens based on tensegrity units that are markedly lightweight and are easily integrated with solar panels and/or sound-proof panels. These units are controlled by tensioning and releasing appropriate cables of the structure and are used to direct the solar panels towards the sun. A mechanical study on the use of tensegrity systems for the design of energy efficient sunscreens inspired by the dynamic solar façades of the Al Bahar Towers in Abu Dhabi is presented. The adaptive architecture of the Al Bahar tower façade is reinterpreted through a tensegrity approach that can change its shape by reacting to the surrounding environment; it is a modern and cost-effective reinterpretation of traditional "mashrabiya" shading systems.

By considering the state of the art on dynamic solar shading systems, all the examples we will examine in Part 1.2 have a major disadvantage which consists in the high cost of the technologies involved. Therefore, buildings with high energy efficiency must be efficient also in terms of the functioning of the building facade, not only in terms of protecting the building from sunlight. So, to respond to this limitation, we were motivated to investigate a new technology that develops dynamic facades with a more effective and sustainable cost. For this reason, inspired by the dynamic solar facades of the Al Bahar Towers in Abu Dhabi, we have studied a tensegrity solution for the "Al Bahar Screen" (ABS) module because it has a morphing behavior that adapts to a comparison with the tensegrity architecture. We label the sun screen designed in the present work as the "Tensegrity Al Bahar Screen" (TABS).

The elements of innovation present in the research project are many and refer to the following points:

i) the application of tensegrity gratings for the design of high energy efficiency solar screens, a research field so far little studied but highly innovative;

ii) modeling of the static analysis of the proposed tensegrity module and extension of this analysis to the dynamic regime, through a "in-house" numerical code;

iii) the addition of wind energy collection units "D-bars" which leads us to the design of the new module labeled WTABS (materials and methods section);

iv) the inclusion of a dynamic modeling of wind forces acting on the proposed screen;

v) the development of a detailed study on the energy collection technology of the WTABS module.

The general objective of the research project was to produce the necessary knowledge to favor the use of the tensegrity architecture in the EEBs field and to guarantee the activation of all those processes related to the innovation of dynamic shading systems. As mentioned above, nowadays there are new performance requirements related to energy efficiency that directly affect proportional new technological proposals and façade solutions consistent with technical regulations on energy consumption containment.

The specific objective was to define a tensegrity solar screen module capable of unfolding thanks to a mechanized system capable of containing energy consumption for heating and cooling, guaranteeing thermo-hygrometric comfort throughout the year and at the same time reducing the environmental impact of the entire building.

The present project deals with the design and control of a special class of Energy Efficient Buildings (EEBs), which exploit the structural paradigm “tensegrity” at different levels (primary and secondary structures) in order to respond to the natural environment by changing their mechanical and HVAC properties.

A tensegrity structure (or system) consists of a rigid body system (tensegrity configuration), usually loaded in compression, which is stabilized through the insertion of prestressed tensile cables (or strings) between the elements. Some of the main advantages deriving from the use of tensegrity architectures in EEBs are the following:

1. it has been shown that the tensegrity architecture provides minimal mass structures for a variety of loading conditions, including structures subject to cantilevered bending load; compressive load; tensile load (under given stiffness constraints); torsion load; and simply supported boundary conditions (e.g. a bridge), without yielding and buckling [21]-[23];
2. the special ability of the tensegrity architecture in integrating control functions within the design of the structure: in controlled tensegrity systems the mechanics of the controller and the structure can naturally cooperate, through the *change* of the configurational equilibrium of the structure, as opposed to traditional control systems, where often the control pushes *against* the equilibrium of the structure;
3. the possibility to look at a tensegrity building as a multiscale sensor/actuator, which in particular features highly nonlinear dynamical behavior, and supports energy transfer through compact solitary waves [24]-[27];
4. the possibility to harvest energy from the environment (such as, e.g., wind and seismic energy), through the conversion of the mechanical energy stored in the structure into electric energy [29],[31];
5. the possibility to construct controllable tensegrity façades, wings, and ventilated walls around the building [28];
6. the easy integration of tensegrity structures with solar and acoustical panels, which can be identified with special rigid members of the structure [28],[29].

This research proposes a methodology that supports the development of the design, construction and development process of new façade components with tensegrity architecture. The project focuses on the study of constructive, structural, functional, typological and formal aspects related to the design and field testing of "intelligent" façade systems, to be used as components of new-generation energy-saving

buildings. The present thesis shows that tensegrity structural systems can be used as an alternative to traditional lattice systems, in the field of solar façade design.

1.1.3 Outline of thesis

This thesis is developed into four sections. The first part refers to the introduction of the topic, and contains background information about previous researches and provides readers with verbal 'road maps', highlighting the main goals. It was analyzed the state of the art of dynamic solar façades through the direct and indirect acquisition of information relating to dynamic and intelligent envelopes and, in a second phase, to tensegrity technologies, developing criteria for the design of solar screens. Section 2 is focused on the kinematics of a tensegrity sunscreen module inspired by that of the Al Bahar Towers' façade in Abu Dhabi, United Arab Emirates. We developed an analytic formulation of the deformation mapping associated with such an actuation motion, giving rise to a morphing-type behavior; we also estimated the energy required to activate the analyzed shading system, and established a comparison between its weight and that of the original screens. In section 3 we simulate the dynamics of the same shading screens with tensegrity architecture through an in-house developed code that handles rigidity constraints on the deformation of the bars. We present numerical results illustrating the dynamic response of the tensegrity solar façade and its morphing capabilities, with a comparison with the kinematic analysis addressed in previous section. The basic module of the examined screens includes tensegrity units with displacement amplification properties that are equipped with piezoelectric cables. A numerical procedure for the simulation of the dynamic response of the examined sunscreens under arbitrary loading is formulated. The proposed model is employed to study the actuation motion exhibited by the elementary origami module, and its vibrations under the action of wind forces. The peculiar ability of tensegrity shading systems to harvest the mechanical energy stored in the strings is investigated, by drawing comparison with the energy harvesting abilities of photovoltaic panels and microeolic turbines.

Conclusions and future development lines of the present study are presented in section 4. The application of tensegrity architectures to the design of façades for new generation energy efficient buildings is also addressed to future works.

Very important was the initial bibliographic research to identify the existing scientific literature on tensegrity envelopes and structures. The analysis of the state of art was also developed through the knowledge of architectural artifacts made with intelligent solar shading, in order to record the technological innovations of the

component and to assess its real correspondence to the requests of the users. The retrieval of information and documents also took place through participation in seminars or conferences dedicated to the topic, in order to identify in real time, the news and contributions that can be found within the scientific research sector.

1.2 State of the art of dynamic solar façades

In the last few years, researchers and engineers focused their studies also on the technological research of façade systems up to demonstrate the possibility of equipping the surfaces with vertical and horizontal closure solutions, able to guarantee the dynamism that allows them to manage the passing material flows in the same way as a biological organism.

The need to comply with the normative directive regarding the energy efficiency of buildings led the technicians to identify new building practices aimed at implementing the technological features of the façades. Therefore, the building envelope is increasingly considered as a dynamic component capable of positively regulating the incoming and outgoing energy flows from the building.

An efficient or environmentally interactive echo envelope offers a control based on the balance between the external environment and the building with the possibility to manage complex energy flows through changes in the surroundings, the shape of the building, the organization of interior spaces and the configurations and actions of the building envelope. This model manages the exchange of heat through the regulation of fixed or variable attitude devices such as dynamic darkening systems or with manual / automatic control and regulation in relation to the type of users and the complexity of the building. An intelligent, adaptive and interactive architectural component, designed and created to adapt as a real living being to changes in external environmental conditions.

The research program investigates the “Dynamic Building Envelopes” sector and more precisely the technology of shading systems, with the improvement of energy performance as a priority objective. In an initial phase, the study focused on the analysis of the state of the art, while in a second phase the design and modeling of a dynamic façade component was investigated, in relation to the variability of its performance. In relation to the construction characteristics and the operating principles of each dynamic shading system, a typological and technological classification has been carried out in order to present an accurate picture of the subject and define the role of shading systems in architecture.

1.2.1 The role of shading systems in Architecture

Adaptive dynamic façades are considered the last frontier of contemporary architectural research and are increasingly connected to the modeling of new building envelopes to guarantee the reduction of energy requirements. The new technologies are directed towards the modeling of all those components that increase the capacity of the envelope to vary conformation in relation to the flows of thermal energy, light, sound passing through it.

Nowadays, contemporary research is oriented to a different conception of the building envelope, that is no longer seen as a static element but as a permeable and selective dynamic interface that regulates that process of interaction between the internal environmental elements and the external world. A correct design of the building organism must be able to independently guarantee the comfort of its users, or thanks to the spread of computer control systems, such as home automation or artificial intelligence systems that allow the regulation of inhabited spaces even in the absence of human user and guarantee conditions of well-being and comfort.

For several decades solar shading has assumed a secondary role in the building design phase, but today the topic of optimizing sunlight has found renewed interest especially in geographical areas characterized by Mediterranean climatic conditions.

Nowadays, solar shading is one of the indispensable technological elements for a good architectural design. It is now an integral part of every architectural work, from residential to office. In the contemporary architectural panorama there is, to date, a varied series of intelligent façade systems, which have both a technological and an aesthetic function, which are configured as innovative design elements.

The choice of using dynamic solar shading in different architectural works was also aided by an enhancement in the IT and technological tools at the service of the eco-sustainable architecture that facilitated the integration of these systems in the design and execution process.

1.2.2 Dynamic solar façades case studies

1.2.2.1 Institut Du Monde Arabe

One of the most interesting examples of a combination of aspects linked to tradition and the use of technology can be found in the Institut du Monde Arabe in Paris, designed by Jean Nouvel, Pierre Soria, Gilbert Lezénés and Architecture Studio. The south west façade of the building has a rectangular shape and is built using moving polygonal geometric motifs. Such panels are made up of square steel diaphragms

that open and close at each change in time, changing the appearance according to the light. Reflecting Islamic architecture, these masharibya panels create interior spaces using filtered light. Between the panels is housed a system of grids that filter the light flow inside by means of photoelectric cells. The grids reminiscent of latticed screens found on patios and balconies in Arab countries. The geometric motifs are motor-controlled and open or close every hour to adjust the amount of natural light which enters the building. These panels form 240 motorized openings that act as dynamic shading systems. The building houses a museum, a library, an auditorium, a restaurant and offices. Considering the solar radiation of the south-facing façade, a sun protection device was needed to build the shading dynamic system. It is an iconic building that for its time stands as a benchmark for dynamic façades [32],[33].

The innovation of the kinetic façade of the present building consists in the ability to automatically adapt to the context, while from the architectural point of view the reference to the wooden mashrabiyas typical of Arab culture is clearly recognizable.

BUILDINGS DATA	FAÇADE FEATURES
Architect: Jean Nouvel, Pierre Soria, Gilbert Lezénés and Architecture Studio Location: Paris, France Year: 1987 Floor area: 16.894 m^2 Stories: 12 Primary use: Offices and Museum	**Material** Square and polygonal steel diaphragms. **Technology** Grid system that filters the luminous flux inside by means of photoelectric sensors. **Opening mechanism** 240 motor controlled apertures.

Table 1.1: The Institut du Monde Arabe – data and features.

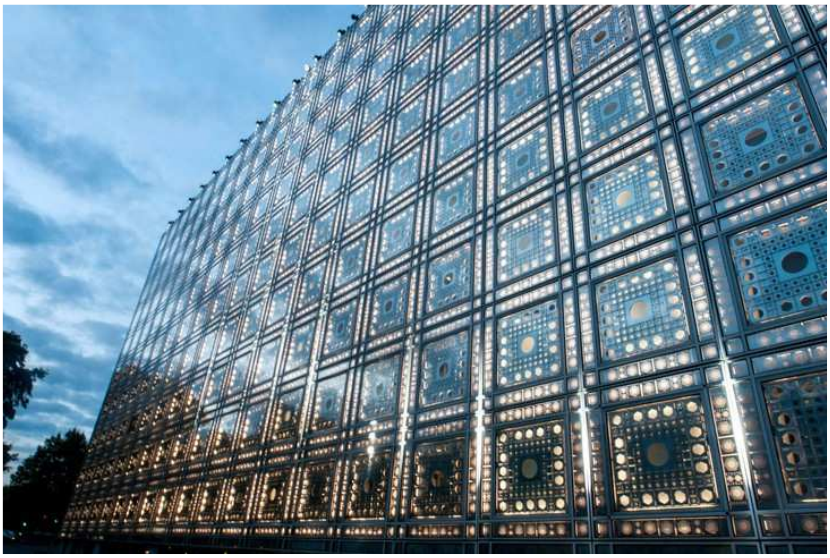

Figure 1.2: The Institut du Monde Arabe façade.

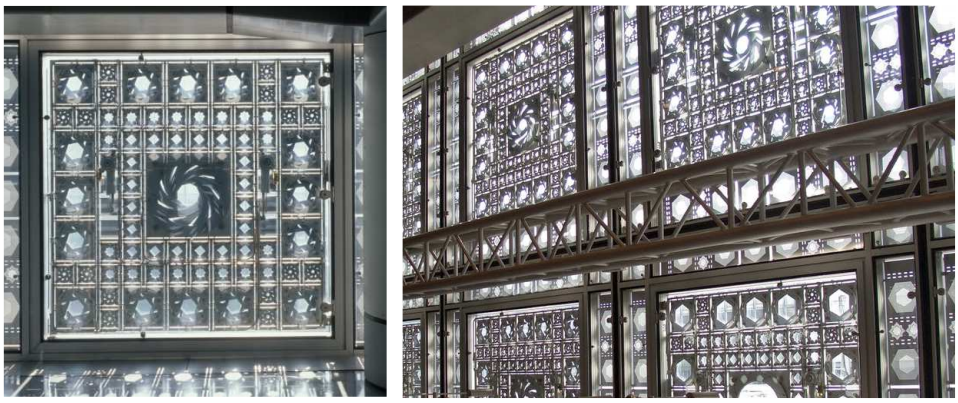

Figure 1.3: The Institut du Monde Arabe – indoor view.

1.2.2.2 RMIT Design HUB

The housing designed by Godsell and Franklin for the RMIT Hub Design is of the double skin type. This building has many different systems related to environmentally friendly design features that refer to waste recycling or water management.

The main feature is the double skin of the Hub that incorporates automated sun-screens that includes photovoltaic cells and systems for evaporative cooling with the

aim of improving the thermo-hygrometric well-being of the internal environment as well as reducing management costs.

The stratification is composed of a curtain wall (curtain wall) of high performance, equipped with double glazing with low-emissivity crystals and air space with argon. At about 700 mm from the curtain wall, anchored to an upright structure in steel profiles, the panels of the second skin are mounted. These are pre-assembled elements in modules of 1.8 meters by 4.2 in height, each consisting of 21 galvanized steel rings (for anti-corrosion protection) buffered by satin-finished glass disks 600 mm in diameter, some fixed, other adjustable [32],[33].

The cells have been designed in such a way that they can be easily replaced and the entire façade of the building can be updated and improved according to the evolution of solar technology, with the aim of obtaining a solar gain that allows costs to be zeroed energy for the entire building.
There is passive cooling to the Underfloor air distribution system (UFAD) consisting of side air intakes and fine mist sprinklers incorporated in the double skin cavity [33].

<table>
<tr><th>BUILDINGS DATA</th><th>FAÇADE FEATURES</th></tr>
<tr><td rowspan="3">Architect: Sean Godsell, Hayley Franklin
Location: RMIT University, Melbourne, Australia
Year: 2012
Floor area: 13.000 m^2
Stories: 9
Primary use: University Institute</td><td>Material
Steel – glass – galvanized steel.</td></tr>
<tr><td>Technology
Façade’s panels with a size of 1.8 by 4.2 meters. These panels consist of a total of 21 glass discs and steel cylinders, which are supported on a secondary galvanized steel frame.</td></tr>
<tr><td>Opening mechanism
12 operable discs and 9 static discs. The movable disks are fitted with an actuator which allows the disks to be exposed to the sun as much as possible.</td></tr>
</table>

Table 1.2: RMIT Design HUB – data and features.

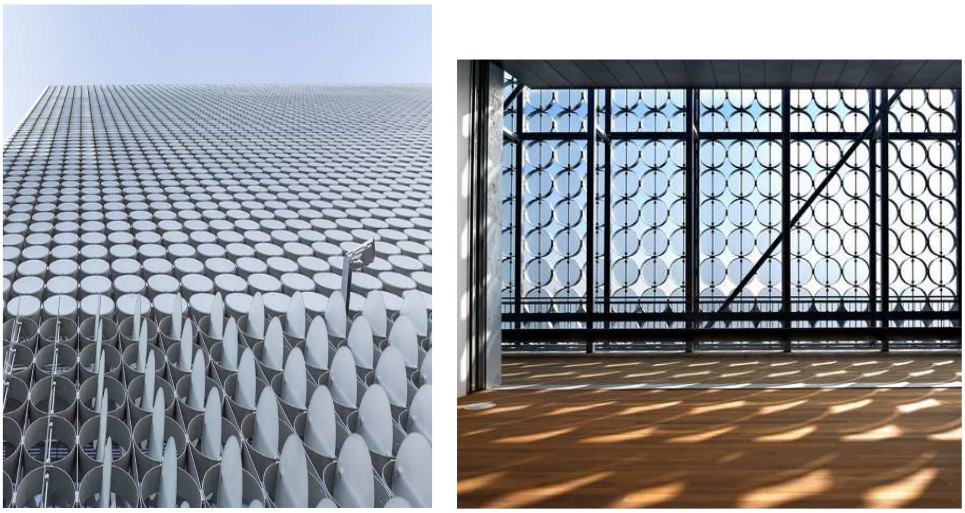

Figure 1.4: RMIT Design HUB – outdoor and indoor view.

1.2.2.3 Council House 2

The Council House 2 is an iconic building, born in Melbourne, to support and raise awareness of sustainable energy in the construction field. The building's façade uses a system of passive energy sources and is composed of timber wooden supported by an aluminum frame. The louvres can be adjusted so as to control the entry of natural light into the building according to the external climatic conditions, protecting the façade from the harsh western sun. The material used for the shutters is untreated recycled wood, while the opening mechanism is controlled by a hydraulic system [32].

The energy efficiency and performance of the building as well as being guaranteed by the dynamic passive façade, also by active intervention strategies connected with the technological support of the plants.

The building is highly energy efficient and is considered an example of green building for the whole of Australia.

BUILDINGS DATA	FAÇADE FEATURES
Architect: Mick Pearce with Designinc Location: Melbourne, Australia Year: 2006	**Material** Timber louvres on an aluminum frame. **Technology**

Floor area: 12.536 m^2 Stories: 10 Primary use: offices	The west facing façade is covered with a system of timber louvres that pivot to optimise the penetration of natural light and views.
	Opening mechanism The louvres are made from untreated recycled timber and are moved by a computer-controlled hydraulic system.

Table 1.3: Council House 2 – data and features.

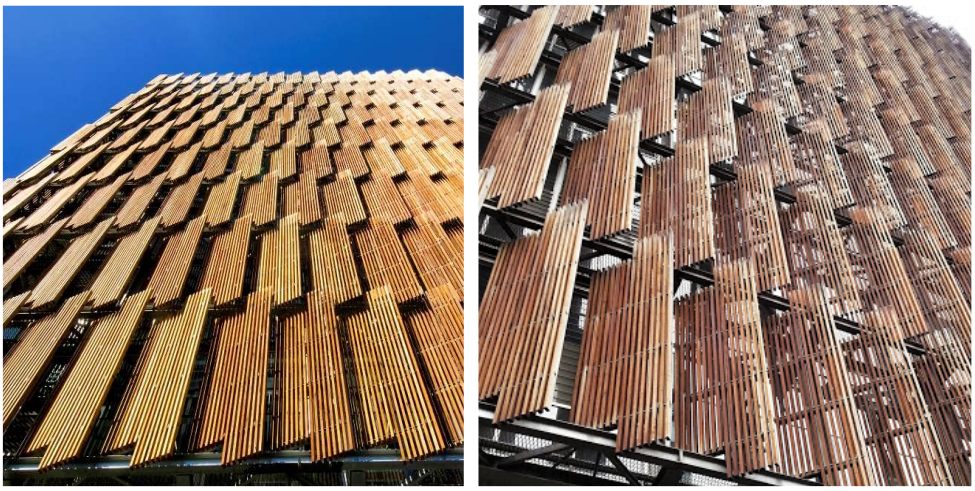

Figure 1.5: Council House 2 – outdoor view.

1.2.2.4 ThyssenKrupp Quarter Essen Q1 building

The solar shading panels play a fundamental role in the design of the façade of the ThyssenKrupp Quarter Essen Q1 building. They are composed of cantilevered elements in adjustable stainless steel, with the aim to improve lighting and climate performance within the offices.

The Q1 building is characterized by two types of façades: an open glass façade in the central space, the other façade faces the L-shaped elements.

The stainless steel sun protection elements consist of approximately 3150 vertical elements and nearly 400,000 bolted horizontal fins. All these rotating and folding elements are driven by the motor and controlled [32],[33].

The elements are all centrally controlled by the engines depending on the position and the solar radiation. This technology allows optimal light control and does not obstruct the view towards the external environment.

The building envelope has a great architectural value thanks to the composition of polygonal darkening elements that create plays of light and artistic effects.

BUILDINGS DATA	FAÇADE FEATURES
Architect: JSWD Architekten + Chaix & Morel Location: Essen, Germany Year: 2010 Floor area: 170,000 m^2 Stories: 14 Primary use: Offices	**Material** Stainless steel.
	Technology The stainless steel sunscreen elements consist of approximately 3150 vertical elements and nearly 400,000 horizontal slats bolted into them.
	Opening mechanism All of these rotating and foldable elements are engine driven and controlled.

Table 1.4: ThyssenKrupp Quarter Essen Q1 building – data and features.

Figure 1.6: ThyssenKrupp Quarter Essen Q1 building – outdoor view.

1.2.2.5 The Pola Ginza building

The building has a double-glazed façade with dynamic panels that can move both horizontally and rotate on themselves.

The sunlight acquired from outside involves the increase in air temperature which is released by the chimney effect on the upper part of the building. This phenomenon allows a stable indoor climate to be maintained and can be adjusted by the users thanks to the windows positioned in the upper and lower part of the double-skin façade that can close or open depending on thermal requirements.

Thanks to the kinetic façade this building is able to react in real time to the climate and optimize energy performance. This system has been shown to reduce annual HVAC energy by 30% [k].

The building's façade is considered a real living organism. It consists of polycarbonate elements with LED lighting capable of creating scenic color effects inside the glazed panels. For each floor there are fourteen panels with automatic hinges positioned to rotate the panels along their curved profile, creating the advantage of having a very compact façade [32],[33].

BUILDINGS DATA	FAÇADE FEATURES
Architect: Nikken Sekkei + Yasuda Atelier Location: Tokyo Year: 2009 Floor area: 35.497 m^2 Stories: 12 Primary use: Offices	**Material** Double glazing and polycarbonate panels.
	Technology The façade is made of a double glazing system and between the glass are kinetic polycarbonate panels with LED lighting.
	Opening mechanism They operate in a group of 14 panels with automatic hinges placed on their tops and the horizontal shaft with rollers that push the panels along their curved profile.

Table 1.5: The Pola Ginza building – data and features.

Figure 1.7: The Pola Ginza building – outdoor view.

1.2.2.6 Kiefer Technic Showroom

The Kiefer exhibition space is located in Bad Gleichenberg in Austria. The building is mainly used as a showroom for the Kiefer Technic company and is nicknamed the

"dancing façade" as it manages to create various types of dynamic movements. The building has a high aesthetic impact and the advantage for the user is the automatic control of the dynamic panels.

The façade is made with aluminum uprights and crossbars. The panels are EIFS façade in white plaster and can be steplessly moved in all three dimensions. The solar screen moves, contracting vertically on electronic shutters of aluminum panels thanks to 56 motors and an intelligent control system. While the air interspace between the two façade layers acts as a climate buffer ensuring an additional insulating layer [32],[33].

Each panel is individually controllable by a touch screen through the users to allow maximum freedom.

The kinetic façade is an intelligent solar shading system, where the user can control the opening/closing of the panels according to the intensity of the sun's rays. Moreover, the folding panels give the façade a third dimension and therefore a different configuration of the shape of the casing.

BUILDINGS DATA	FAÇADE FEATURES
Architect: Ernst Giselbrecht + Partner Location: Steiermark, Austria Year: 2007 Floor area: 545 m^2 Stories: 12 Primary use: Offices	**Material** Aluminum posts and Exterior Insulation and Finish System (EIFS)-façade transoms encased in white plaster.
	Technology 112 perforated aluminum panels that are electronically controlled by 56 motors.
	Opening mechanism Sliding mechanism.

Table 1.6: Kiefer Technic Showroom – data and features.

Figure 1.8: Kiefer Technic Showroom – outdoor view.

1.2.2.7 Soka-Bau Building Offices

The Soka-Bau Building have been designed with smart façade of extremely high performance to reduce fossil energy consumption. It's composed by highly insulated and user-controllable wooden panels in each module of the façade.

The south and north façades are characterized by dynamic sun-shaded panels with a concave shape that represent a distinctive feature of the entire building. These elements are made of highly reflective aluminum sheet for deflection of sunlight and are hooked to powder-coated aluminum brackets. On the façade of the north side these panels are fixed and reflect the zenithal light on the internal ceiling, while on the south side are constituted by mobile elements in concave aluminum and regulate the entry of natural light. The activation mechanism consists of a motor with a lifting spindle. Moreover, the presence of two metal reinforcing elements ensures the sunshade profile strength for the purposes of safety and protection of the rooms.

In addition to the dynamic shading system, other measures have also been adopted to ensure high comfort with low energy values such as triple glazed windows, free natural ventilation, study of solar intensity on workstations and recycled materials [32],[34],[35].

BUILDINGS DATA	FAÇADE FEATURES
	Material Blasted stainless – extruded sheet-aluminum - light refracting glass.
Architect: HERZOG + PARTNERS Location: Wiesbaden, Germany Year: 2003 Building area: 170 m x 108 m Stories: 5 Primary use: Multi-use building	**Technology** Concave louvers reflects direct sunlight in the required quantities into the room. The lower wing moves down to shade the lower part of the façade. A light-deflection panel was fixed to the balconies to direct zenith-light into the back of the rooms.
	Opening mechanism Spindle hoisting motor.

Table 1.7: Soka-Bau Building Offices – data and features.

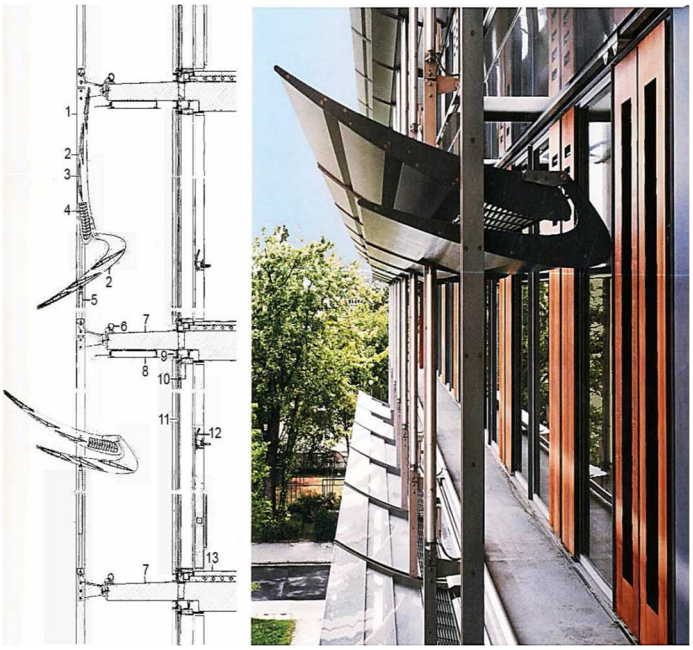

Figure 1.9: Soka-Bau Building Offices – outdoor view.

1.2.2.8 The Al Bahar Towers

The Al Bahar Towers are located in Abu Dhabi. The city experiences a warm and humid climate with a temperature that reaches, in extreme cases, 48°C, while 100% humidity, during the summer, reason why the building envelope technology plays a major role in this context.

The project of the innovative Al Bahar towers was born following an international competition launched by the Abu Dhabi Investment Council in 2008.

The big problem in the Arabic countries climate is the solar gain caused by large glazed façades of the buildings. This aspect is present in the Al Bahar Towers where the design brief consists in a cylindrical form to offer a Golfo Persico better view with a façade that is open in all directions. Therefore, the most advanced interactive solar façade system has been designed. The heart of the Al Bahar tower project consists of a modern reinterpretation of the traditional "mashrabiya" shading façade, a passive cooling system typical of the areas of the Arab world, consisting of grids, with a more or less dense texture, in able to reduce the effects of high ambient temperatures and intense solar radiation. The result is an iconic building that combines a contemporary design with a strong appeal to traditional Islamic architecture. Mashrabya shading devices, consisting of perforated wooden trellis screens with sundry geometric patterns that perform multiple functions (grating privacy, reducing solar gain and protecting the inhabitants from glare) and are able to guarantee thermo-hygrometric well-being. The sunscreen module proposed by the design team consists of a scalable hexagon that acts as a solar barrier and responds dynamically to the position of the sun. The opening and closing of these panels is automatically controlled by computers to respond to optimal solar and light conditions.

The activation of the module is driven by a electric linear actuator which is centrally located and it is based on a low energy consumption technology. Each module consists in six deployable panels and has height of 4200 mm whit a width ranging between 3600 mm and 5400 mm. The panels can be deployed for a free opening area of 85% thanks to a maximum piston-actuated stroke of up to 1000 mm. Each shading module weighs about 1.5 tonnes for a total of 1049 modules for each tower. The indoor vision area of the curtain wall spans 3100 mm. Each Al Bahar screen module was conceived as a single shading system, anchored to a substructure by means of movement joints, with a cantilevering of 2.8 m from the primary structure.

The support structure consists of duplex stainless steel support frames and dynamic elements anchored in aluminum with fiberglass mesh infill. Each panel is covered

by polytetrafluoroethylene (PTFE) material. Each module is driven by an automated motor with a pre-programmed sequence and it is protected by sensors that react to external weather conditions by opening the panels in the events of overcast conditions or high winds [36]-[38].

BUILDINGS DATA	FAÇADE FEATURES
Architect: Mick Pearce with Designinc Location: Melbourne, Australia Year: 2006 Floor area: 12.536 m^2 Stories: 10 Primary use: offices	**Material** Timber louvres on an aluminum frame.
	Technology The west facing façade is covered with a system of timber louvres that pivot to optimise the penetration of natural light and views.
	Opening mechanism The louvres are made from untreated recycled timber and are moved by a computer-controlled hydraulic system.

Table 1.8: The Al Bahar Towers – data and features.

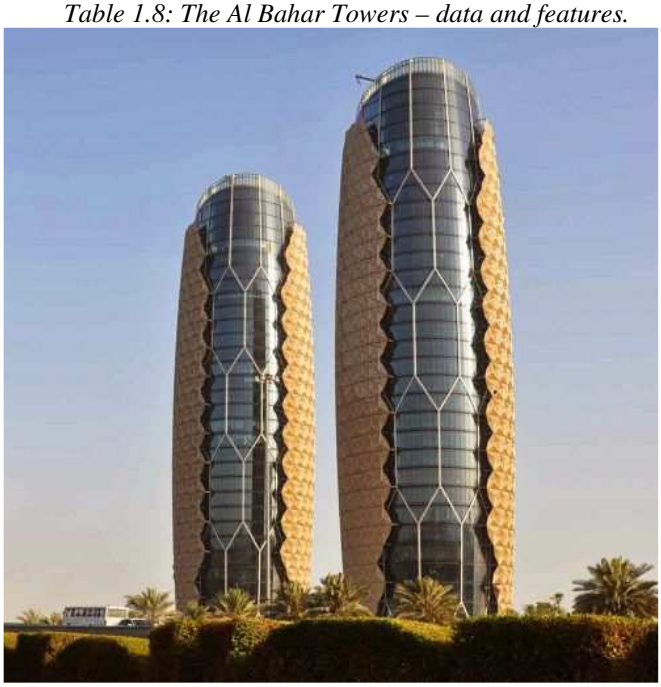

Figure 1.10: The Al Bahar Towers – outdoor view.

1.3 Tensegrity systems

1.3.1 Basic principles

Since the 1950s, the tensegrity system has officially been recognized as a new construction technique. The main innovative aspect of this technology is the understanding of the static balance of the isolated bars. For a long time, the basic principle of construction has always been the same: the balance of the building is guaranteed thanks to the weight of the structure, that is, through compressive forces of vertical elements that transmit the weight of the building to the ground. However, the tensegrity structures are based on a completely different approach: structural stability is guaranteed by the creation of an autonomous state of equilibrium through compressed rods and cables in traction and therefore does not need the gravitational principle to be in equilibrium. The continuous discontinuous compression / traction system is the fundamental characteristic of these structures and provides unique properties compared to most civil engineering works. To better understand the tensegrity principle, we report below some mechanical and structural analogies. Actually, several authors admit that inflatable constructions are tensegrity because they are self-balanced systems composed of an external traction component that embraces the gas atoms which behave like discontinuous elements in compression.

The most ancient example of tensegrity structure can be probably found in the kite. This primitive toy is made up of two crossed sticks and a tight rope that, by connecting the ends of the sticks, identifies the four sides of the element. This typology is basically a two-dimensional structure and, presenting two compression rods that touch each other, it cannot be defined as a pure tensegrity. It is not a coincidence that Snelson conceived the first tensegrity sculpture starting from the kite modules [39].

1.3.2 The form-finding problem

Depending on the type of struts used by the tensegrity system, different tensegrity classes are identified, each of which is characterized by a greater mechanical stiffness than the previous class.

Systems that provide for the presence of only one compressed element per node, are defined as class 1 tensegrity structures (pure tensegrity); systems that require the presence of 2 compressed elements converging in a single node are called class 2 tensegrities; systems of 3 elements converging into a single node are called

tensegrity class 3, and so forth. The same Fuller [40] created a class 4 tower, made up precisely of modules composed of 4 rigid bars welded together at one end.

Resistance to external stresses in a tensegrity system is mainly dependent on two factors: the geometric and topological conformation of the elements, and the value of the pretension applied to the strings (Fig. 1.11).

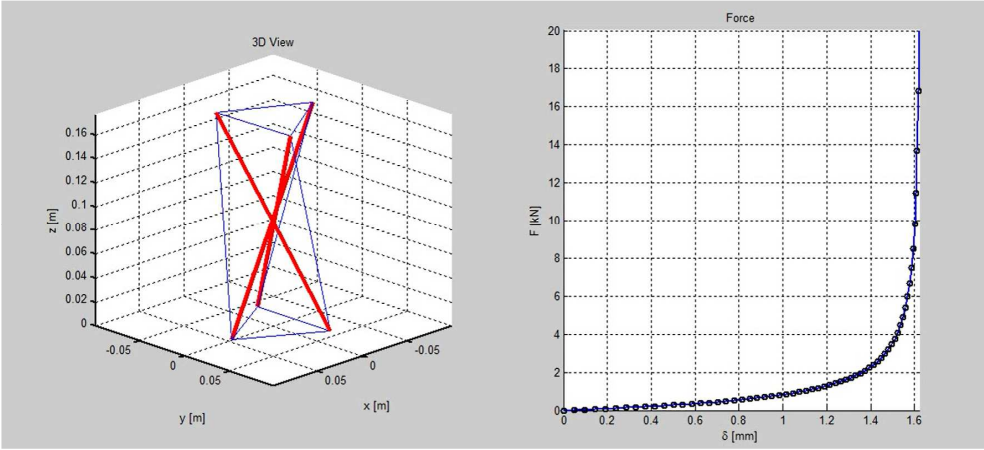

Figure 1.11: Reduction of sagging in a tensegrity prism according to pre-stress.

Researches have shown that class 2 tensegrity structures, which present two bars in contact for each node, are more stable and statically more efficient than class 1 structures, in which the rods float in a vacuum [41]. Furthermore, the efficiency of tensegrity structures in relation to the load / mass load ratio was highlighted; it has been pointed out that, compared to a reticular structure composed of rigid elements, tensegrity systems are less efficient, while under certain loading conditions they can be slightly more efficient than a continuous linear element. In such structures, the resistance to external loads is non-linear and varies, even a lot, depending on the type of the applied load; in general, it can be affirmed that all tensegrity structures show a strong drop in strength when only one of the cables composing them becomes loose. This in some cases represents the collapse of the structure and it is therefore one of the parameters to be taken into account during the design and dimensioning phases. If it is not possible to act on the shape of the system to counter the effect of the applied forces, then it is possible to act on the pre-tensioning. This concept is among the fundamentals for discerning true tensegrity systems from what they are not.

As stated by R. Motro [42] of the University of Montepellier: "It is called tensegrity a system in a state of stable self-equilibrium comprising a discontinuous series of

compressed components within a continuum of thesis components". We can also affirm that in general tensegrity systems are spatial reticular structures, formed by compressed components (rods) and tensile elements (cables), which are in a state of self-equilibrium, in which the compressed components are inside the structure defined by the network of tensile elements. With this, it is understood that, having identified the external shape of the system (its edges) they must be traversed exclusively by the stretched ropes, while the compressed struts can have the ends on the edges. Every other point belonging to them must remain inside of the limits marked by the ropes.

State of self-equilibrium means that the structure is stable and maintain its shape with zero external loads, including its own weight. Stability is defined as the ability of a system to return to its initial position after a perturbation, this definition allows any possibility, it is worth as much for tensegrities as for membranes and not only, it also admits the use of fluids (air). The analogy with an inflatable structure previously mentioned is very useful to explain the concept of pre-stress. For example, a balloon can be in three different states: deflated; swollen with no internal pressure; swollen with some internal pressure. In the first case, it is evident that the ball has no particular shape, or better if it is stimulated by external forces, it can assume an unspecified number of forms, so it is possible to affirm that it is in a non-stable state. In the second case, the balloon takes its shape, because the volume of air inside it is exactly equal to the volume that the ball is able to contain, however, prompted by external actions it is not able to maintain its conformation, because it does not it has no rigidity. In the third case, instead, more air is introduced inside the balloon than the balloon is able to contain and this generates an internal pressure; this internal pressure can be seen as a constant force of compression acting on the walls of the balloon, which in turn to withstand this thrust are in a state of tension. This condition puts the outer membrane of the balloon in a condition of pre-stress regardless of the application or otherwise of external stresses; at the same time, it is precisely this pre-stress induced state that makes the balloon reactive to external actions and therefore stable, ie capable, if disturbed, of returning to the initial state.

In tensegrity structures, the stabilizing force is given by the lengthening of the struts or by the shortening of the tie rods. If the length of the struts is too short or the length of the tie-rods is too long the system is cinematically indeterminate, as it can assume innumerable configurations. There exists one and only one length of the elements such that the structure finds itself in an equilibrium condition with zero pre-stress; in this condition the system is once again cinematically indeterminate, but this time the internal mechanism is infinitesimal. From this point on, if we try to lengthen the

struts or shorten the rods, then we impose a state of internal pre-stress on the system that stabilizes the structure and makes it resilient to external actions, stabilizing in some cases even the infinitesimal internal mechanisms also called second order kinematics [43]. The pre-stress value can vary within a range that if exceeded leads to the collapse of the structure or due to failure of the tie-rods or failure of the struts.

1.3.3 Features

Tensegrity structures can be defined as transformable structures, this means that tensegrities are able to change their three-dimensional configuration. However, this transformation must not compromise efficiency and be autonomous and repeatable. The lightness of tensegrity systems, modularity, and the presence of compressed elements hinged together make these structures definable as folding. This ability is considered to be of fundamental importance, as it facilitates the transport and storage of the elements. The most interesting examples in which it has been taken advantage of the folding/unfolding properties of these structures, come from the field of space applications. In fact, dimensions, lightness and transport costs have greater relevance for aerospace scopes. Research in this field has been carried out by the works of Tibert and Motro [42].

1.3.3.1 Properties

This subsection will list the main advantages and disadvantages of the tensegrity structures that have been identified following research and theoretical and laboratory studies [44]. The main properties of tensegrity structures include:

- Lightness: compared to other structures, with a similar resistance and at the same load conditions, they are very light. Tensegrity structures provide minimal mass systems for different loading conditions.

- Modularity: they can be designed to be modular. Elementary tensegrity cells can be joined together to create different shapes, grids or plans made by their union or by the union of different elements.

- They are suitable for dry assembly. The components are joined with mechanical joining technologies and made solid without the use of connection materials destined to consolidate after laying, such as adhesives and sealants. This reduces construction time and guarantees a high level of flexibility.

- Synergy: the behavior of the entire system does not foresee the behavior of one of their components taken separately. They have the ability to respond as a whole, so local stresses are transmitted uniformly and absorbed throughout the structure.

- Auto-stability: they are auto-stable. Tensegrity structures don't depend on gravity due to their self-stability, therefore they do not need mandatory anchor constraints and can be placed on any surface.

- As they are reticular structures, they do not have a cut, bending moment and torque.

- From the structural point of view, they can be compared to three-dimensional reticular structures, therefore they are not subject to shear stress, bending moment and torque.

- The load-bearing capacity of the tensegrity systems is directly proportional to the self-stress level. And the degree of tension of the prestressed components is proportional to the amount of space they occupy.

- Fractal property: tensegrity structures can be divided into a greater number of modules. The use of fractal geometries in the framework of tensegrity structure search methods derives from the use of a finite or infinite number of repetitions of elementary modular geometries.

- They are not subject to high instability loads since the compressed elements are discontinuous and work only locally.

- The rigidity of the structure depends on the materials used, and their method of assembly. They can be very flexible or very rigid and very strong.

- Deployability and foldability: they can be deployed and folded by adjusting a limited number of elements (strings).

- The response to loads is non-linear. The stiffness increases with increasing load.

- Enantiomorphism: there is an inverse equality that is concretized in symmetry with respect to a plane, so that one of the two entities can be considered as the mirror image of the other. Symmetrical pairs are formed

in both directions.

1.3.4 Tensegrity sistems in EEBs

A civil structural system is composed by the design of: structures; HVAC (heating, ventilating and air conditioning) system; electrical system; sighting design; etc. Such systems have traditionally been designed in the order listed, in sequence. Modern building technology must be more efficient, both in construction and in operation.
It is well known that energy saving is of great importance nowadays, because of the increasing cost of raw materials and the growing energy demand of developing countries. Especially in geographical areas that have insufficient natural resources, new buildings should be able to significantly minimize energy consumption, while existing buildings should undergo energy efficiency retrofits. Energy efficiency can be achieved by minimizing heat and air conditioning consumption on the one hand, and making use of energy harvesting techniques from renewable sources (solar, wind, geothermal) on the other.

The building of the future also needs to be safer with respect to natural hazards, such as earthquakes and high winds, and more energy efficient in terms of making components and subsystems multidisciplinary (e.g. combining HVAC and structural design).

Techniques are not yet available to integrate these disciplines, which have previously been separated into a sequence of disciplines, applied one at a time. The structure of such a building should be designed to respond to its environment with respect to thermal energy, acoustic energy, earthquake energy, wind energy, etc. The structure of such a building should be designed to respond to its environment with respect to thermal energy, acoustic energy, earthquake energy, wind energy, etc. Actually all of these issues should be integrated into a single optimization problem, or feasible constrain problem with bounds specified for motion (deflection at joints), thermal bounds, acoustic attenuation, energy bounds for control and power consumption.

The present project deals with the design and control of a special class of Energy Efficient Buildings (EEBs), which exploit the structural paradigm “tensegrity” at different levels (primary and secondary structures) in order to respond to the natural environment by changing their mechanical and HVAC properties.

In the field of Energy Efficient Buildings there are several advantages deriving from the use of tensegrity systems. In particular, these structures provide minimal mass elements for different loading conditions, including structures subject to cantilevered bending load; compressive load; tensile load (under given stiffness constraints);

torsion load; and simply supported boundary conditions (e.g. a bridge), without yielding and buckling [21]-[23]; they can harvest energy from the environment (wind or seismic energy), through the conversion of the mechanical energy stored in the stings elements into electric energy [29],[31], or the possibility to harvest solar energy through the easy integration of these structures with photovoltaic panels, which can be identified with special rigid members of the structure [28],[29].

Tensegrity structures can be adapted for the construction of controllable tensegrity façades, wings, or natural ventilated walls around the building envelope [28]; moreover, in tensegrity structures, the mechanics of the unfolding process and the overall structure are connected by the configurational change of the structure and this guarantees an optimal control in the design of the structural system, unlike the traditional typologies where the control pushes against the equilibrium of the structure. This property is closely linked to the capacity of the tensegrity lattices to operate as multiscale actuators thanks to their highly non-linear dynamic behavior capable of transferring energy through compact solitary waves [24]-[27];

Part II. On the kinematics of a tensegrity sunscreen module

We refer to the shading façade designed by Aedas architects as the "Al Bahar Screen" (ABS) throughout this thesis.
The tensegrity solution that we propose for the re-design of the ABS controls the tension in selected cables forming the shading structure. It is aimed at demonstrating that the use of tensegrity concepts for the design of active solar façades leads to lightweight morphing systems that require minimal storage of internal energy and reduced operation costs. Such a design can easily be generalized to dynamic skins of energy efficient buildings featuring different topologies, upon retaining the use of morphing architectures [52], and deployment mechanisms controlled through cable stretching and relaxation [28]. We label the sun screen designed in the present work as the "Tensegrity Al Bahar Screen" (TABS).
The structure of this chapter is as follows. We begin by reviewing the AHR design of the ABS in chapter 2.1. Next, we move on to design a basic TABS module, by developing an analytic formulation of the kinematics of such a structure.
We prove that the employed actuation mechanism requires the deformation of a limited number of members, and exhibits a morphing-type response (chapter 2.2). The stress analysis of the TABS module is conducted in chapter 2.3, while an estimate of the energy costs associated with its actuation is presented in chapter 2.4.

2.1 A review of the ABS module

2.1.1 The Al Bahar Towers design

The biggest challenge that contemporary architecture has to address, in order to make progress in sustainability, is to optimize natural resources and minimize energy consumption. To provide the best answer to this need it is necessary to design flexible and reconfigurable building envelopes able to dynamically react on the base of the evolution of weather and environmental conditions (Figure 2.1). The adaptive architecture of the Al Bahar tower façade by AHR develops a new design approach based on structural systems that can change their shape by reacting to the surrounding environment. The heart of the Al Bahar tower project consists of a modern-day reinterpretation of the traditional "mashrabiya" shading system.

The latter is a passive shading technology typical of the Arab world, which consist of perforated wooden screens forming wonderful geometric patterns, which reduce solar gain and mitigate air conditioning consumption resulting from direct exposure to solar rays [37].

The peculiarity of the adaptive ABS consists in no longer interpreting the mashrabiya as a static and two-dimensional system, but rather as a façade design approach generating three-dimensional origami shapes (Figure 2.1B), whose motion in space can be controlled by sensors and actuators during daylight hours (typically, from 9 a.m. through 5 p.m.) [45]. The evaluation of the insulation property of a façade, the so-called U-value (defined as the amount of heat passing per unit of surface of the screen, under one Kelvin temperature gradient between indoor and outdoor), is a topic of paramount interest for the architects and engineers operating in the field. Energy studies conducted on the ABS lead to conclude that the overall U-value of this building envelope is equal to 2.0 W/m^2K, which corresponds to that of a solid brick wall (Designing BuildingsWiki)[1]. The origami panels are covered by a polytetrafluoroethylene (PTFE) coated fibermesh, which reduces the G-value of the façade more than 50% (i.e., the ratio between the total solar heat gain and the incident solar radiation), as compared to a glazed envelope [38]. The activation of the ABS is driven by a centrally positioned electric screw-jack linear actuator (piston-actuated computer-controlled technology) that operates on low energy consumption.

The linear actuator stroke reaches up to 1,000 mm, which folds the panels and provides up to 85% clear opening area [37] (Figure 2.1C). The structural elements of the ABS are made of duplex (austenitic-ferritic) stainless steel supporting frames and Aluminum dynamic frames, with each triangle of the screen covered by a glass fiber panel (Figure 2.1B) [38],[47]. The umbrella-like module of the ABS has a height of 4,200 mm, and a width ranging between 3,600 and 5,400 mm. In total, each tower has 1,049 shading modules, each weighing a 1.5 tons [37],[47].

[1] Available online at: https://www.designingbuildings.co.uk/wiki/U-values.

Figure 2.1: (A) Illustration of the Al Bahar towers in Abu Dhabi. (B) detail of a module of the ABS (picture taken during the mounting of the screens). (C) ABS actuation mechanism (reproduced with permission from Karanouh and Kerber, 2015).

2.2 Kinematics of the TABS module

The TABS concept is illustrated in Figure 2.2, with reference to a basic module of the structure. The analyzed module is composed of six "micro-triangles," and is such that its boundary forms a "macro-triangle" when projected onto a plane parallel of the building façade (umbrella-like module). The activation mechanism of the TABS module is driven by a linear actuator, which stretches the perimeter strings, by pushing against a vertex of the macro-triangle along its bisector, in parallel to the building façade. The mechanism is guided by two linear springs controlling the in-plane displacements of the other two vertices of the macro-triangle, and a telescopic collar guiding the out-of-plane displacement of the center of mass of the module (Figure 2.2). It is worth remarking that such a "tangentially" activated mechanism substantially differs from that driving the ABS module, since the latter pushes orthogonally to the building façade, against the center of mass of the module [37],[38],[47]. We study in chapter 2.2.1 the existence of a deformation mapping of the TABS module, which corresponds to the described actuation mechanisms and ensures that all the micro-triangles move rigidly in space. Such a morphing-type behavior [52],[53] induces minimal storage of internal energy during the actuation phase, and ensures high stiffness and stability when the actuation mechanism is not triggered (cf. chapters 2.3, 2.4).

The model of the TABS adopted in following analytical and numerical developments is reported in Figure 2.3, to which we refer for notation. The module is described as a tensegrity system formed by 3 strings parallel to the building façade and aligned with the edges of the macrotriangle (red-colored members), and 12 bars forming the edges of the micro-triangles (black-colored members). Figure 2.3 depicts the

completely folded configuration (Figure 2.3A) of the tensegrity model, which we assume as reference, and the unfolded, perfectly flat configuration (Figure 2.3B). The TABS model is formed by seven nodes (numbered from 0 to 6 in Figure 3), for a total of 21 degrees of freedom (ndof = 21). The adopted Cartesian frame is reported in Figure 2.3.

In agreement with the activation mechanism described above, the boundary conditions (BCs) of the TABS module are as follows:

$$\begin{aligned}
&\text{on node 0:} \quad u_{0(x)} = 0;\ u_{0(y)} = 0;\\
&\text{on node 2:} \quad u_{2(x)} = 0;\ u_{2(z)} = 0;\\
&\text{on node 4:} \quad u_{4(y)} = \frac{u_{4(x)}}{\sqrt{3}};\ u_{4(z)} = 0;\\
&\text{on node 6:} \quad u_{6(y)} = -\frac{u_{6(x)}}{\sqrt{3}};\ u_{6(z)} = 0;
\end{aligned} \tag{2.1}$$

where $u_i(x)$, $u_i(y)$ and $u_i(z)$ are the Cartesian components of the nodal displacement vector $\mathbf{u}_i$ exhibited by the generic node i. The BCs (2.1) must be complemented by three additional equations, respectively associated with the linear actuator acting on node 2, and the two springs acting on nodes 4 and 6 (actuation constraints, cf. Chapter 2.2.1).

2.2.1 Rigid body transformation

Let us investigate on the existence of a rigid body transformation of the TABS deprived of external constraints, which cause stretching (positive) strains only in the perimeter strings connecting nodes 2, 4, and 6 (cf. Figure 2.3), measured from the fully-folded configuration (rest configuration), while keeping all the bars undeformed. The rigid-body deformation mapping under investigation is constrained by the 11 BCs defined above, plus 12 rigidity constraints associated with the bars forming the module. In agreement with BCs (2.1), the displacement vector of node 2 attached to the linear actuator of the TABS module is given by

$$\mathbf{u}_2 = U\mathbf{e}_y, \qquad U \geq 0, \tag{2.2}$$

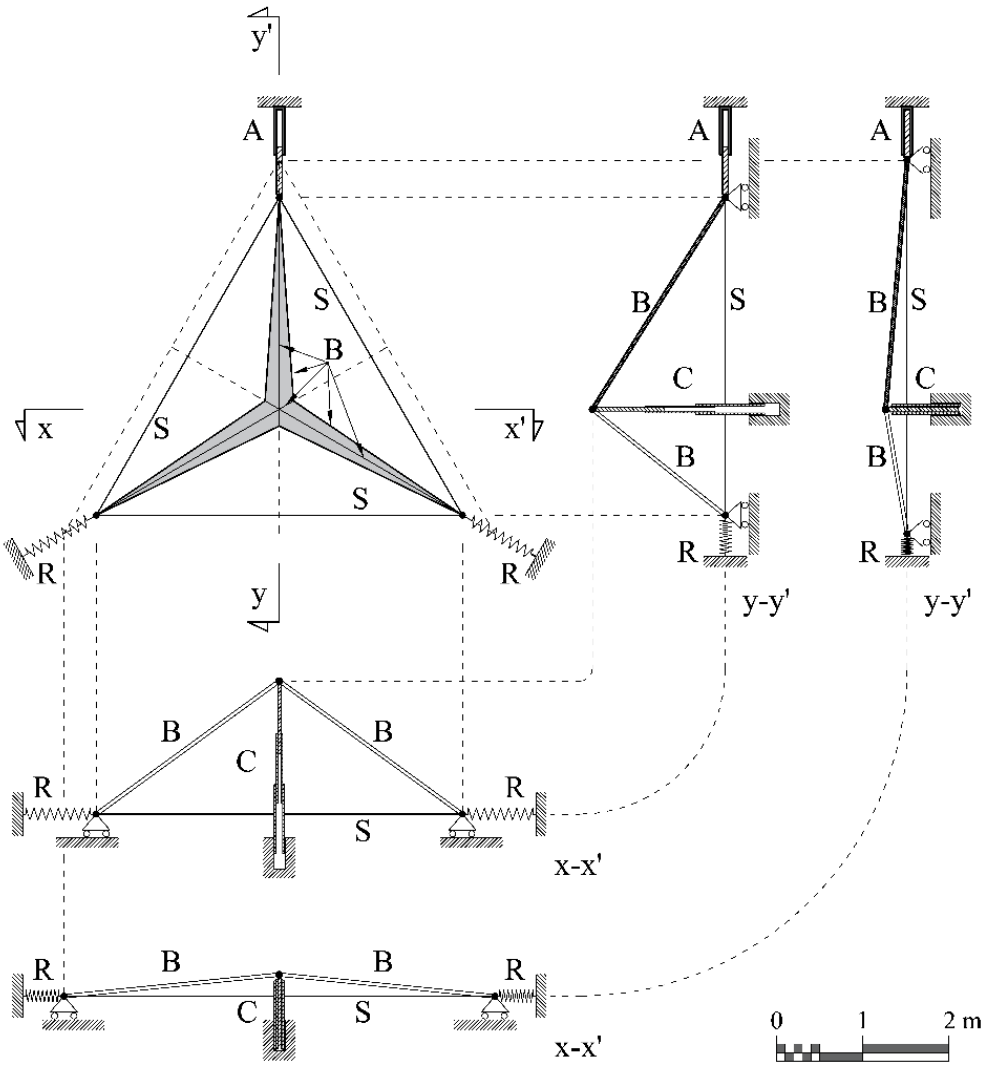

Figure 2.2: Schematic views of the TABS concept: top view and mid-plane sections (in two different configurations): A, linear actuator; B, bars; C, telescopic collar; R, elastic restraints; S, perimeter strings. Restraints are idealized and not reported in scale.

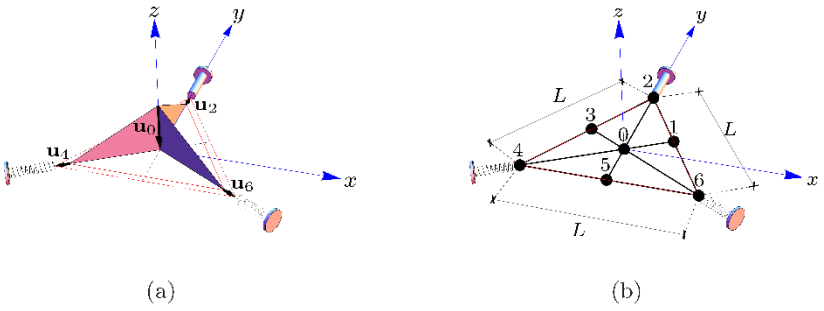

Figure 2.3: Reference (A) and deformed (B) configurations of a tensegrity model of the TABS module. (A) shows the folded configuration of the structure corresponding to the fully opened screen. (B) depicts the flat configuration (fully closed screen), where the module reduces to an equilateral triangle with side L. Nodes 2, 4, and 6 are mutually connected through deformable strings (red-colored members), which are at rest in the reference configuration, and fully stretched in the flat configuration. The strings are superimposed to the perimeter bars in the flat configuration (B).

U denoting the time-dependent norm of such a displacement, which is measured from the fully folded configuration. Due to constructive needs, we require that the researched rigid body transformation is such that the displacements of nodes 4 and 6 exhibit the same norm U of u_2 (due to symmetry), and nodes 5, 3, and 1, respectively move along the y-axis (i.e., the projected 5–2 edge onto x, y-plane, see Figure 2.2), the projected 3–6 edge (aligned with the y-axis rotated of $\pi/3$), and the projected 1–4 edge (aligned with the y-axis rotated of $-\pi/3$).

Our next developments will show that such assumptions are equivalent to the enforcement of the actuation constraints at the vertices of the TABS module. Overall, the deformation mapping associated with the researched rigid body transformation of the TABS is described by Equation (2.2), and the following additional displacement laws

$$\mathbf{u}_0 = -\alpha \mathbf{e}_z, \tag{2.3}$$

$$\mathbf{u}_1 = \frac{\sqrt{3}\beta}{2}\mathbf{e}_x - \frac{\beta}{2}\mathbf{e}_y + \gamma \mathbf{e}_z, \tag{2.4}$$

where α, β, and γ are unknown functions of U, to be determined on enforcing rigidity constraints on all the bars. In the completely folded and flat configurations it trivially results

$$\alpha = 0, \quad \beta = 0 \quad \text{and} \quad \gamma = 0 \qquad \text{for} \quad U = 0 \tag{2.5}$$

$$\alpha = \frac{L\sqrt{3}}{6}, \quad \beta = 1 \quad \text{and} \quad \gamma = 0 \qquad \text{for} \quad U = \overline{U} = \frac{2\sqrt{3}-3}{6}L \tag{2.6}$$

Let us label the position vectors of the generic point i in reference and deformed configurations as $\mathbf{X}_i$ and $\mathbf{x}_i$, respectively. The rest and deformed lengths of the e^{th} element attached to nodes *i* and *j* are given by

$$L_e = \sqrt{\left(\mathbf{X}_i - \mathbf{X}_j\right)\cdot\left(\mathbf{X}_i - \mathbf{X}_j\right)}, \tag{2.7}$$

$$l_e = \sqrt{\left(\mathbf{x}_i - \mathbf{x}_j\right)\cdot\left(\mathbf{x}_i - \mathbf{x}_j\right)}, \tag{2.8}$$

where dot symbol $(\cdot)$ denotes the scalar product between vectors. The rigidity constraints to be considered require that it results

$$L_e^2 = l_e^2, \tag{2.9}$$

in correspondence to all the bars (here, squared lengths are used for algebraic convenience). It is easily shown that the enforcement of such constraints leads us to the following system of three independent (nonlinear) equations

$$\begin{aligned} &3\alpha^2 - \sqrt{3}L\alpha + 3LU + 3U^2 = 0, \\ &3(\alpha+\gamma)^2 - \sqrt{3}L(\alpha+\gamma) + 3\beta^2 = 0, \\ &2\beta^2 + 2\gamma^2 - L\beta - 2U\beta + 2LU + 2U^2 = 0, \end{aligned} \tag{2.10}$$

which admit four distinct sets of solutions for α, β and γ, as it can be verified through the use of the `Solve` function of *Mathematica*®. Three of such solutions violate Equations (2.5) and (2.6), while the unique admissible solution has the following expression

$$\begin{aligned} \alpha &= \frac{L - \sqrt{L^2 - 12LU - 12U^2}}{2\sqrt{3}}, \\ \beta &= \frac{2LU}{L - 6U}, \\ \gamma &= \frac{\sqrt{3}U\sqrt{L^2 - 12LU - 12U^2}}{L - 6U}. \end{aligned} \tag{2.11}$$

We are therefore led to the following expression of the 7×3 matrix $\hat{x}(U)$ that collects the deformed coordinates of nodes from 0 to 6 of the TABS module,

$$\hat{x} = \begin{pmatrix} 0 & 0 & \frac{\sqrt{L^2 - 12LU - 12U^2}}{2\sqrt{3}} \\ \frac{\sqrt{3}LU}{L-6U} & \frac{LU}{L-6U} & \frac{-\sqrt{3}U\sqrt{L^2 - 12LU - 12U^2}}{L-6U} \\ 0 & U + \frac{L}{2} & 0 \\ -\frac{\sqrt{3}LU}{L-6U} & \frac{LU}{L-6U} & \frac{-\sqrt{3}U\sqrt{L^2 - 12LU - 12U^2}}{L-6U} \\ -\frac{\sqrt{3}}{4}(L+2U) & -\frac{1}{4}(L+2U) & 0 \\ 0 & -\frac{2LU}{L-6U} & \frac{-\sqrt{3}U\sqrt{L^2 - 12LU - 12U^2}}{L-6U} \\ \frac{\sqrt{3}}{4}(L+2U) & -\frac{1}{4}(L+2U) & 0 \end{pmatrix} \tag{2.12}$$

Equation (2.12) gives the analytic description of the researched actuation motion of the TABS module. Graphic illustrations of such a transformation are provided in Figures 2.4–2.6, on assuming L = 4.55 m, as in the ABS [38], and the displacement U of the actuated node as order parameter. It is worth noting that the elongation (i.e., the change in length) exhibited by the perimeter strings is equal to $\sqrt{3}U$, which corresponds to the engineering strain $\varepsilon = 2U/L$. For $U = \overline{U}$ (perfectly flat configuration) the engineering strain exhibited by the perimeter strings is considerably high, and approximately equal to 15%. In correspondence to the examined value of L, it is immediate to verify that it results that $\overline{U} = 0.352$ m, and that the norm u_0 of the out-of-plane displacement of node 0 is equal to 1.313 m (unfolding displacement of the umbrella module). Figure 2.4 shows that the mid nodes 1, 3, and 5 of the edges of the macro triangle exhibit negative z-displacements, which implies that such nodes move toward the building façade during the actuation of the TABS (cf. also Figure 2.6). It is useful to compute the minimum value of the z displacement of such nodes during the TABS actuation, with aim of sizing the gap to be allowed between such a structure and the building façade. Making use of Equation (12) and the Solve function of *Mathematica*®, it is not difficult to verify that it results $du_{1(z)}/dU = 0$ for $U = U^\circ = 0.059$ L, and $u_{1(z)\min} = -0.079\ L$. In particular, for $L = 4.55$ m, one gets $U^\circ = 0.268$ m, and $u_{1(z)\min} = -0.359$ m. We

therefore conclude that the TABS module must be placed at least at ~ 36 cm from the building façade. It is worth noting that the Aedas design of the Al Bahar Towers places the ABS at 2.8 m from the façade of the towers, for window cleaning and shading system maintenance [37],[47].

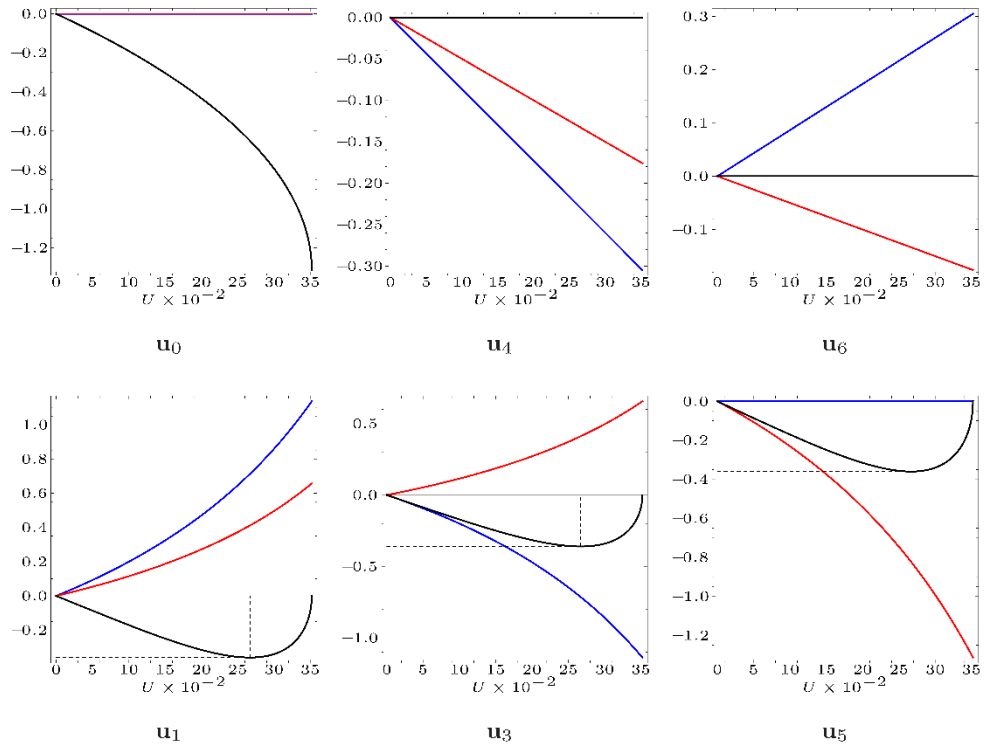

Figure 2.4: Nodal displacements from the fully folded configuration exhibited by the non-actuated nodes of the TABS module, assuming L = 4.55 m. The Cartesian components of the nodal displacements along the x-axis are marked in blue, while the components along the y-axis are marked in red, and those along the z-axis are marked in black.

2.3 Stress analysis of TABS

The present Chapter is devoted to the computation of the axial forces carried by the members of the TABS model under the actuation motion (chapter 4.1), and wind-induced forces (chapter 4.2). For the sake of simplicity, and considering the common operation times of the analyzed sun [37],[38],[47], we assume that the TABS structure reacts to such loading conditions through a quasi-static deformation process, by neglecting inertial and damping (i.e., dynamical) effects. Upon extending the mechanical theory presented in [57],[60] to the TABS model under

consideration, we describe the generic member of such a structure as a linear spring that carries an axial force t_e obeying the following constitutive law

$$t_e = k_e \left(l_e + L_e \right), \tag{2.13}$$

where it results

$$k_e = \frac{E_e A_e}{L_e}, \tag{2.14}$$

Ee denoting the Young's modulus of the material, and Ae denoting the cross section area.

Our physical model of the TABS assumes L = 4,550 mm (cf. Chapter 3.1), and makes use of Aluminum alloy hollow tubes for the bars and nylon-fiber ropes for the strings, whose properties are given in Tables 2.1, 2.2, respectively. Aluminum bars were chosen because of their lightweight nature and high corrosion resistance [58], while nylon-fiber ropes were selected due to the fact that such elements combine a considerably low Young's modulus, elastic elongation to failure (or yield strain) slightly greater than the deformation needed for actuation purposes (≈15%, cf. Chapter 3.1), and considerably high tensile strength (see Table 2..2, where the given mechanical properties have been imported from a web source, 2018[2]; refer, e.g., to [62] for fabrication information). Other possible choices for the strings of the TABS may employ suitable natural or artificial fibers (see [61] and references therein), or rubber materials [68]. The adopted physical model adequately approximates the rigid-elastic response analyzed in chapter 3.1 (rigid bars and flexible strings), since it includes bars exhibiting axial stiffness much greater than the axial stiffness of the strings (E_bA_b = 493.625 E_sA_s, subscripts b and s denoting bars and strings, respectively, see Tables 2.1, 2.2). The total potential energy of the TABS model under consideration is given by

$$\Pi = \frac{1}{2} \sum_{e=1}^{n} t_e \left(l_e - L_e \right) + \frac{K}{2} \left(u_{4(x)}^2 + u_{6(x)}^2 \right), \tag{2.15}$$

where K denotes the stiffness of the actuation springs applied to nodes 4 and 6 (cf. Figure 2) that we assume equal to 67 kN m^{-1} ($K = E_sA_s/L$). The equilibrium equations of the TABS model under arbitrarily large nodal displacements $\hat{u}_j$ (j = 1, ..., ndof)

[2] http://publica.fraunhofer.de/documents/N-161087.html.

are obtained by imposing stationarity of the total potential energy (Equation 15) with respect to such quantities, which leads us the following system of equations

$$r_j = \frac{\partial \Pi}{\partial \hat{u}_j} = \sum_{e=1}^{n} t_e \frac{\partial l_e}{\partial \hat{u}_j} \hat{\lambda} w_j = 0, \quad j = 1,..., n_{\text{dof}}. \tag{2.16}$$

Here, the index e runs from one to the total number of members m, which include bars, perimeter strings and actuation springs, while the quantity $\hat{\lambda}$ denotes a scalarmultiplier of the nodal forces w_j (j = 1, ..., ndof).

We computed the solution of the nonlinear system (Equation 16) through the path-following algorithm described in Mascolo et al. (2018) [57], with reference to two distinct deformation processes. The first process is aimed at estimating the mechanical response of the examined physical model under the actuation motion studied in chapter 3.1 (cf. Chapter 4.1).
In the second process, the structure is deployed from the fully-folded configuration to the almost closed configuration corresponding to U = 0.95 $\overline{\text{U}}$, and next is subject to wind-forces acting on such a configuration (cf. Chapter 2.3.2). The reason for applying wind forces on the configuration with U = 0.95 $\overline{\text{U}}$ (instead of the fully flat configuration corresponding to U = $\overline{\text{U}}$) is two-fold, technological and aesthetic. From a technological point of view, we note that the fully flat configuration of the TABS module is not completely deployable, due to the finite size of the bars forming such a system, which unavoidably get in touch before the configuration with U = $\overline{\text{U}}$ is reached (see Figures 2.1, 2.5). Regarding aesthetic issues, we observed that having a technologically closed" configuration of the TABS module, which is not perfectly flat, ensures that such a structure has an origami shape in correspondence to all the steps of the actuation motion (cf. Figures 2.5, 2.6), as in the original ABS design [37],[47].

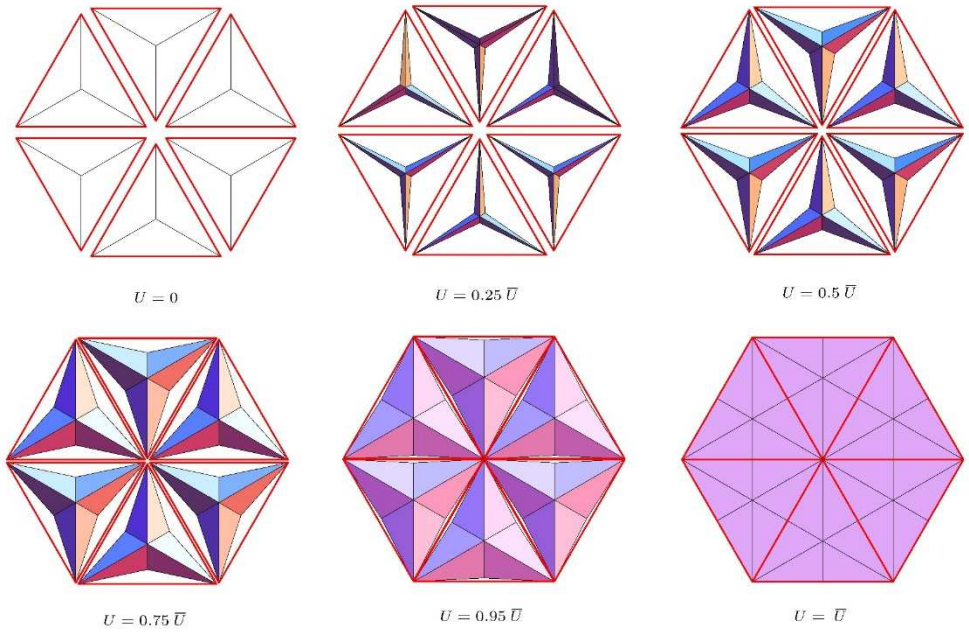

Figure 2.5: Top views of a TABS compound in six different states. Shortening L of actuator strings corresponding to each state is reported.

2.3.1 Forces and stresses induced by the actuation process

Let us focus our attention on the forces carried by the perimeter strings in correspondence with the fully-flat configuration with $U = \overline{U}$, and the almost closed configuration with $U = 0.95\ \overline{U}$, alongside the actuation motion of the TABS. It is an easy task to compute such quantities using the path-following algorithm described in [57], or, alternatively, by simply observing that the elongation of the perimeter strings is equal to $\sqrt{3}U$ in the generic, deformed configuration of the TABS (cf. Chapter 3.1). The forces, strains and stresses carried by the perimeter strings in the above configurations of the TABS are shown in Table 2.3. It is immediate to verify that the stresses carried by the strings in correspondence to the analyzed configurations, are slightly lower than the tensile strength of 616 MPa of the adopted nylon-fiber ropes (cf. Table 2.2).

The use of the path-following procedure outlined in chapter 4 leads us to obtain the nodal forces acting on the TABS module for $U = \overline{U}$ and $U = 0.95\ \overline{U}$, which are shown in Table 2.4.

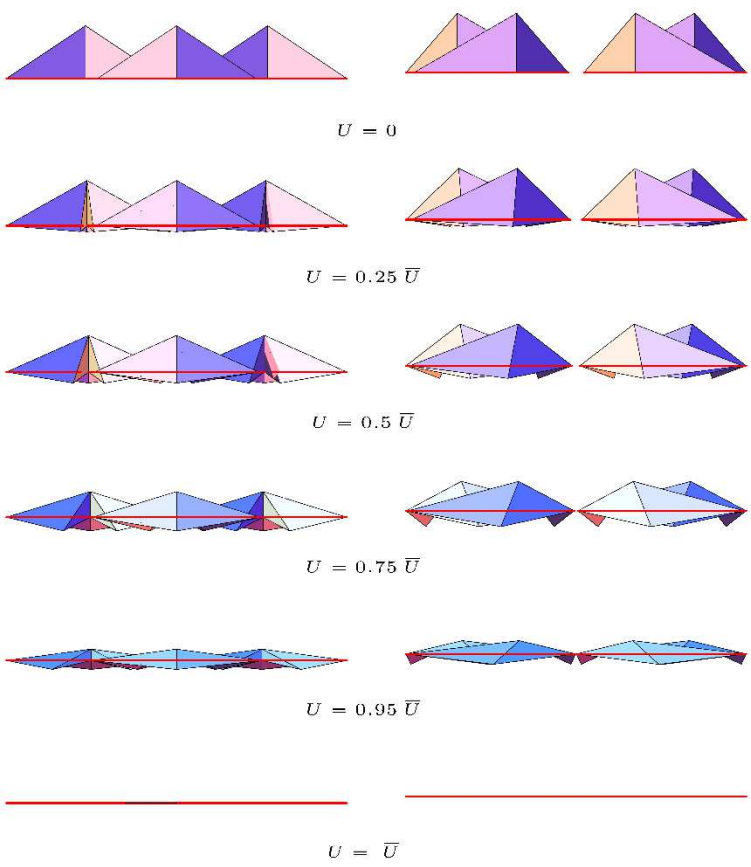

Figure 2.6: Side views of different frames of the TABS actuation motion).

Table 2.1: Geometric and mechanical data of 6082-T5 Aluminum bars.

Width	Height	Thickness	Material	Young's modulus	Density	Yield Stress	Yield strain
ω (mm)	h (mm)	t (mm)		E_b (GPa)	ρ (kg/m^3)	σ (MPa)	ε_b (%)
150	70	5	6082-T5	72	2.70x10^3	260	0.2

The force acting on the node 2 will be employed in chapter 5 to select the linear actuator to be applied to the TABS module under consideration.

2.3.2 Effects of wind loading

Relevant external loads for the stress analysis of the TABS are those induced by the action of positive and negative (i.e., suction) wind pressures on the closed configuration of the structure [38]. It is known that wind induces dynamic, intrinsically random, and time-dependent loads on wind-exposed structures, whose direction is variable in time and influenced by a number of different factors (refer, e.g., to the European standard for wind actions EN 1991-1-4, 2005).

By addressing a dynamical treatment of wind forces on the TABS to future work, in the present study we focused our attention on the equivalent static wind load analysis, which is contemplated by technical standards (EN 1991-1-4, 2005 [51]; [48]). We considered a fixed direction of wind forces parallel to the z-axis of the adopted Cartesian frame (Figure 2.3).

Table 2.2: Geometric and mechanical (effective) data of (nylon-fiber ropes).

Diameter	Material	Young's modulus
d (mm)		E_s (GPa)
10	Nylon ropes	3.9

Density	Yield Stress	Yield strain
ρ_s (kg/m^3)	σ_s (MPa)	ε_b (%)
1.14x10^3	616	15.8

Table 2.3: Strain, stress and axial force carried by the generic perimeter string in the almost fully-flat (U = 0.95 $\overline{U}$) and fully-flat (U = $\overline{U}$) configurations.

$U=\overline{U}$		
Strain	Stress	Axial Force
ε (%)	σ_S (MPa)	N (kN)
15.4	598.255	46.987
$U=U$		
Strain	Stress	Axial Force
ε (%)	σ_S (MPa)	N (kN)
14.6	568.657	44.662

Table 2.4: Nodal forces acting in the almost fully-flat (U = 0.95 U) and fully-flat (U = U) configurations.

	$U=0.95\overline{U}$			$U=\overline{U}$		
Node	R_x	R_y	R_z	R_x	R_y	R_z
	(kN)	(kN)	(kN)	(kN)	(kN)	(kN)
0	0	-297.975	0	0	-313.723	0
2	0	276.167	-25.318	0	290.759	-11.024
4	19.286	10.904	12.659	20.304	11.482	5.512
6	-19.286	10.904	12.659	-20.304	11.482	5.512

Table 2.5: Strains, stresses and axial forces produced by the application of positive wind pressure forces on the TABS configuration corresponding to U = 0.95$\overline{U}$.

Element	Strain	Strass	Axial force	Buckiling load
	ε	σ_s	N	N_b
	(%)	(MPa)	(kN)	(kN)
1-0	0.000	0.105	0.221	−728.031
2-0	0.080	57.462	120.669	−182.008
2-1	0.025	17.758	37.292	−242.677
3-0	0.000	0.105	0.221	−728.031
2-3	0.025	17.758	37.292	-242.677
4-0	-0.010	−78.954	−165.803	−182.008
4-3	0.025	17.757	37.290	-242.677
5-0	0.000	0.091	0.192	−728.031
4-5	0.023	16.786	35.250	-242.677
6-0	−0.010	−78.954	−165.803	−182.008
6-5	0.023	16.786	35.250	-242.677
6-1	0.025	17.757	37.290	-242.677
2-6	14.586	568.868	44.680	0
6-4	14.476	564.569	44.341	0
4-2	14.586	568.868	44.680	0

Table 2.6: Strains, stresses and axial forces produced by the application of negative wind pressure forces on the TABS configuration corresponding to U = 0.95 $\overline{U}$.

Element	Strain ε (%)	Strass σ_s (MPa)	Axial force N (kN)	Buckiling load N_b (kN)
1-0	0.000	−0.247	−0.519	−728.031
2-0	0.177	127.276	267.279	−182.008
2-1	-0.025	−18.285	−38.399	−242.677
3-0	0.000	−0.247	−0.519	−728.031
2-3	−0.025	−18.285	−38.399	-242.677
4-0	−0.021	−15.435	−32.414	−182.008
4-3	−0.025	−18.284	−38.394	-242.677
5-0	0.000	−0.226	−0.475	−728.031
4-5	−0.024	−17.143	−36.000	242.677
6-0	−0.021	−15.435	−32.414	−182.008
6-5	−0.024	−17.143	−36.000	-242.677
6-1	−0.025	−18.284	−38.396	-242.677
2-6	14.581	568.665	44.663	0
6-4	14.466	564.163	44.309	0
4-2	14.581	568.665	44.663	0

Making use of the results of wind tunnel tests on full-scale prototypes of the ABS presented in [38] e [47], we assumed the wind pressure $\hat{\lambda}$ = 3.5 kPa over the projection of the screen onto the x, y-plane. Said $\|\cdot\|$ the Euclidean vector norm, × the vector product symbol, and introduced two vectors $\mathbf{a}_p$ and $\mathbf{b}_p$ lying along the edges of the generic micro-triangle (or panel) forming the TABS, the surface area A_p of such an element was computed as follows

$$A_p = \frac{1}{2}\left\|a_p \times b_p\right\|, \tag{2.17}$$

while its unit normal is given by

$$n_p = \frac{a_p \times b_p}{\left\|a_p \times b_p\right\|}. \tag{2.18}$$

The wind force acting over the generic panel p, along its normal vector, was computed through ([48],[51])

$$\omega_p = \hat{\lambda} A_p \left(\mathbf{n}_p \otimes \mathbf{n}_p \right) e_z, \tag{2.19}$$

ez denoting the unit vector along the z-axis, and $\otimes$ denoting the tensor product symbol. The wind force acting on the generic node of the TABS was finally obtained as follows

$$w_i = \frac{1}{3} \sum_{p=1}^{n_i} \omega_p, \tag{2.20}$$

n_i denoting the number of panels attached to node i. As already anticipated, we applied both positive and negative wind pressure forces on the almost flat configuration of the TABS corresponding to $U = 0.95\,\overline{U}$. An application of the path-following algorithm described in [57] lead us to the results reported in Tables 2.5, 2.6, which show the axial strains, stresses and forces carried by all the members of the TABS module under such loading conditions, assuming tensile strains, stresses and forces as positive. The results shown in Tables 2.5, 2.6 highlight that the stresses carried by the strings and bars are lower than the corresponding yield strengths, and that the axial forces carried by the bars, when negative, are lower than the local Eulerian buckling loads. In particular, the axial stresses carried by the bars are significantly lower than the yield stress of 260 MPa. We accept that the bars can be loaded either in compression (negative bar forces) or in tension (positive bar forces), while we require that the strings must always work in tension. Tables 2.3, 2.5, and 2.6 show that the strings of the TABS module (members 2– 6, 6–4, and 4–2) always carry positive forces. This is due to the actuation mechanism of the module, which leads the strings to be fully stressed under a tensile strain of the order of 15% in the (theoretically) fully closed configuration of the screen. It is worth remarking that the marked stretching of the strings in the closed configuration of the system, confers significant geometric stiffness [28] to such elements, preventing them from going slack, e.g, under the action of suction wind forces.

2.3.3 Aeroelastic stability of the tabs module

Light-weight structures are exposed to aeroelastic effects, that is, fluid-structure interaction phenomena that occur when the displacements and/or velocities of the structure are such as to alter, in a non-negligible way, the wind pressure range. The main aeroelastic phenomena that can influence the TABS module examined in the present study are galloping and divergence. The first is an aeroelastic phenomenon characterized by the cancellation of the damping of the structure. It is a dynamic

instability that regards structures and slender elements, not very heavy and equipped with a small ratio of structural damping, characterized by cross sections of non-circular shape that, under certain conditions, can manifest transversal oscillations of great amplitude. The phenomenon is possible, even for modest speeds, for all cables, whose cross section can be modified by the presence of a layer of ice.

The divergence, on the other hand, is an aeroelastic phenomenon characterized by the cancellation of torsional stiffness. It is a static type instability that regards structures characterized by a flattened shape in the direction of the incident flow and by an intrinsic weakness in the torsion actions. The phenomenon can involve thin and flexible structures, such as aluminum panels, anchored to the TABS module.
Galloping oscillation starts at a special onset wind velocity $v_{G,i}$ and normally the amplitudes increase rapidly with increasing wind velocity.
The onset critical wind velocity of galloping, $v_{G,i}$, is given by [EN 1991-1-4 2005: Eurocode 1] [51]:

$$v_{G,i} = \frac{2 \cdot n_{L,i} \cdot b \cdot S_{C,i}}{a_G} \tag{2.21}$$

In order to exclude the instability by galloping, or make its occurrence highly unlikely, it is necessary to satisfy the condition $v_{G,i} > v_{m,l}$, where $v_{m,l}$=90.00 m/s (value used in reference). In general, the most severe condition concerns the first mode of vibration. The critical galloping speed for the first transverse vibration mode, $v_{G,1}$, is given by Eq. (7) where $m_{e,1}$=28.35 kg/m is the equivalent mass m_e per unit length for mode i (value related to the Scruton module), $n_{L,1}$=14.1 Hz is the cross-wind fundamental frequency of the structure, $\varepsilon_{L,1}$=0.001 is the factor of structural damping, ρ=1.25 kg/m^3 is the density of the air, b=0.55 m. Furthermore, the Scruton number relative to the first transverse vibration mode is S_{c1}=58.16. Finally, the instability factor for galloping is assumed to be a_G=0.7 (the section of the considered element is included in Eurocode Table). Therefore, $v_{G,I}$ = 92.02 m/s > $v_{m,l}$ = 90.00 m/s.

It should be noted that based on this result, the test for galloping appears to be satisfied under limit conditions. More accurate checks could be obtained by wind tunnel tests on full-scale TABS prototypes.

The divergence phenomenon is achieved when the wind speed v_m is equal to the critical velocity of divergence v_D. For the benefit of security, to avoid instability due to divergence, it must satisfy the following condition: $v_D > 1{,}2 \cdot v_{ml}$.

Where the critical wind velocity for divergence is given by:

$$v_D = \sqrt{-\frac{2 \cdot G \cdot J_t}{\rho \cdot d^2 \cdot c'_{mZ}}} \tag{2.22}$$

with:

G = 26GPa (modulus of rigidity).
ρ = 1.25 kg/m^3 (density of the air).
J_t =1.17x10^{-5} m^4 (moment of torsional inertia of the cross section).
d=1.67 m (in wind depth (chord) of the structure)
$c'_{mZ} = d_{cM}/d\Theta$ =-1.65 (values are measured about the geometric centre of various rectangular sections depending on the ratio b/d).
Therefore, results: v_D = 325.22 m/s > 1,2· v_{ml} = 90.00 m/s.

2.4 Energy cost and weight

2.4.1 Energy consumption and weight estimation

The present Section is primarily devoted to estimate the energy cost associated with the operation of the linear actuator applied to node 2 (see Figure 2.3) of the system illustrated in Figure 2.2. We begin by sizing such an actuator, using a commercially available, electro-mechanical actuator of the Rolaram® series by Power Jacks (2018). The activation force (or dynamic load) prescribed to the actuator is assumed coincident with the nodal force computed at node 2 of the configuration with U = 0.95 $\overline{U}$, which is equal to Fa = 290.759 kN (cf. Table 2.4). Table 2.7 shows different Rolaram® actuators ensuring dynamic load capacity of the same order of magnitude of Fa. The activation time of such actuators have been computed through the product of the inverse of the actuation speed by the stroke U = 0.95 $\overline{U}$ ≈ 334 mm, while the corresponding energy consumptions have been computed by multiplying the activation time by the power requested by the actuator.


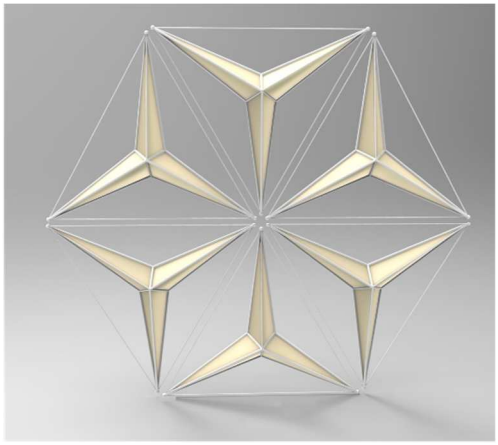

Table 2.7: Graphical comparison between ABS (left) and TABS (right) modules.

The device that is most suited for our scopes in Table 2.7 is the actuator Rolaram® R2501190, which shows 294 kN dynamic loading capacity and maximum stroke of 3,500 mm (Power Jacks, 2018). The activation time of such an actuator, which is required to take the TABS module from the fully folded to the almost flat configuration ($U = 0.95\,\overline{U}$), can be rather short, and approximately equal to 17 s. The corresponding energy consumption is markedly low, equal to that needed to keep a light bulb of 35 W lit for 1 h. Obviously, such an activation time can be suitably relaxed for operational purposes, as a function of the programmed opening and closure times of the screen. We wish to remark that the "parallel" actuation mechanism of the TABS module analyzed in the present work contemplates a stroke that is equal to 33% of that needed to actuate the analogous module of the ABS via a central piston (1,000mm, cf. [38]; [47]).

We close the present section by presenting a comparison between the weight of the examined physical module of the TABS and that of the ABS module designed by Aedas architects [11]. Figure 2.7 shows a graphical comparison of ABS and TABS umbrella modules, highlighting the different sizes of the structural members that form such systems. It is useful to observe that the ABS solution presents different families of bars: primary bars placed behind the screens supporting the actuation mechanism; Aluminum frames supporting the panels; stabilizers connecting the first two sets of bars; and cantilever struts separating the screens from the façade of the towers (see Figure 2.1C, and Figure 17 of [38]). The total weight of the ABS module is reported as approximately equal to 1.5 tons (14.71 kN) in [47] and [37].

The TABS module is instead formed by 12 bars placed along the perimeters of the six micro-triangles forming the system (Figures 2.2, 2.3). The weight of the structural part of the TABS module equipped with Aluminum bars and nylon-fiber ropes (see data in Tables 2.1, 2.2) is easily computed, and amounts to 1.43 kN. We safely doubled such a weight, in order to grossly account for the additional weights of joints, rails, springs and secondary elements. The weight of the infill panels amounts to about 0.13 kN, on using PTFE panels, as in the original ABS design [37],[38],[47], which have self-weight per unit area of 0.015 kN m^{-2} and cover an area of about 9 m^2 per module (see e.g., [70] Structurflex, 2018 for fabrication information). The total weight of the actuator is 4.41 kN, by summing the weight of the selected device (4.23 kN, see Table 2.7) to the weight of 0.18 kN of the roller screw (PowerJacks, 2018). By summing the above weights, we finally estimate the total weight of the TABS module approximately equal to 7.40 kN. It is worth observing that such weight is 50% lower than the ABS weight per module reported in [37].

The greater lightness of the TABS module vs. the corresponding ABS module can be visibly appreciated in Figure 2.7. We don't have numerical data on the energy consumption required by the deployment of the ABS module, which nevertheless is reported to work "on very low energy consumption", too [38]. It is worth noting that the significant reductions of the stroke of the linear actuator and the weight of the TABS module, over the ABS design, are expected to further reduce operation costs and the environmental impact of the system.

Part III. On the dynamics of a tensegrity sunscreen module

3.1 Mechanical modeling of the WTABS dynamics

3.1.1 WTABS Layout

The basic module of the WTABS examined in the present study enriches the TABS unit studied in [36], due to the addition of a set of six D-bar systems acting as mechanical energy harvesters. The original TABS system is graphically illustrated in Fig. 3.1. It is composed of 'origami' (umbrella shaped) eyes, whose unit cell (or basic module) consists of a tensegrity structure formed by 12 bars and 3 perimeter strings. The activation motion of each module is controlled by stretching and relaxing the perimeter strings, which leads to suitably tune the geometric stiffness of the structure [28]. The module is made up of a macro-triangle anchored parallel to the building façade, which is subdivided into six micro-triangles. The latter are able to move rigidly in space according to a morphing-type behaviour, thereby ensuring minimal internal energy storage in the deployment phase.

The elementary module of the WTABS system is shown in Fig. 3.2(b,c). Fig. 2(b) details the six D-bar units added to the TABS module of Fig. 3.2(a), while Fig. 2(c) shows the overall WTABS module. The actuation of such a structure is powered by a linear actuator Rolaram® R2501190 (294 kN dynamic loading, 3500 mm maximum stroke [64]), which is positioned at a vertex of the module. The actuator stretches and relaxes the external cables (see Fig. 3.2(b)), thus activating the unfolding/folding mechanism of the system. A telescopic collar guides the movement of the infill panels along the z axis, orthogonally to the building's façade (Fig. 3.1). Two linear springs with stiffness constant K = 67 kN m^{-1} control the in-plane displacements of the other two vertices of the structure. The module employs 6082-T5 Aluminum bars and nylon fiber ropes as strings, which are subject to axial strains up to $\approx$ 15% [38].

The total weight of the original TABS module is approximately equal to 7.40 kN, including structural parts (about 3.00 kN), PTFE (glass fiber) infill panels (0.13 kN), and the linear actuator (4.23 kN). Such a weight is approximately equal to one half of that of the sunscreens designed by Aedas architects for the Al Bahar towers

[37],[38]. The height of the module is equal to 4200 mm, while its width ranges between 3600 mm and 5400 mm. The bars of the WTABS module are made of the 6082-T5 Aluminum alloy, while the strings have a composite architecture, being formed by a central nylon cable coated by a bundle of Polyvinylidene Fluoride (PVDF) piezoelectric cables [77],[78]. We refer the reader to Chapter 3.4 for the overall mass analysis of the WTABS module, and the mechanical properties of its components.

Figure 3.1: Illustration of the TABS design for the origami sunscreens of the Al Bahar Towers in Abu Dhabi [36].

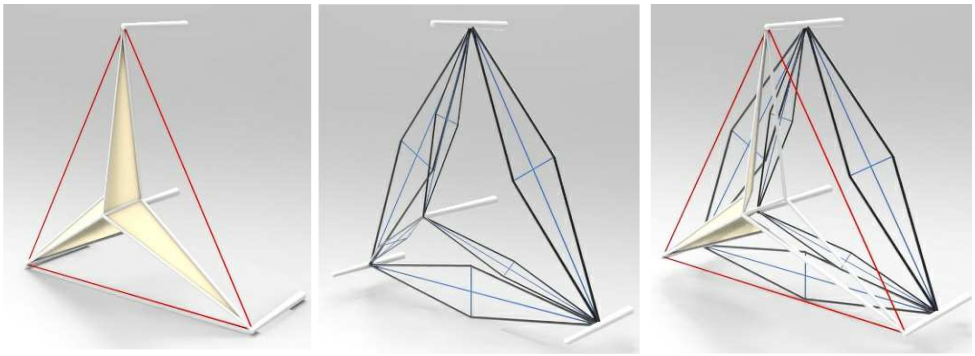

(a) (b) (c)

Figure 3.2: Illustration of the WTABS model: (a) elementary TABS module; (b) D-bar elements with mechanical energy harvesting abilities; (c) overall WTABS module.

3.1.2 Equations of motion

The present section illustrates a numerical model for the simulation of the dynamic response of the WTABS structural system, through a Runge-Kutta approach to the time-integration of the competent equations of motion [79] (Sect. 3.1). The employed procedure suitably generalizes that presented in Refs. [79],[80], in order to account for the presence of wind forces (Sect. 3.1.3).

Throughout the thesis, we indicate matrices with bold capital letters (i.e. **X**), vectors with bold lower case letters (i.e. **x**), and scalars with italic letters (i.e. *x*). The examined mechanical model describes the bars as rigid members and the strings as elastically deformable elements. It is composed of n_n nodes (or joints), n_b bars and n_s strings (or cables), and makes use of the following basic assumptions:

- the strings act as straight elastic springs that can carry only tensile forces (no-compression response);
- the bars behave as straight rigid bodies with uniform mass density, constant cross-section, and negligible rotational inertia about the longitudinal axis [79];
- the nodes consist of frictionless ball joints;
- duplicated nodes are introduced in correspondence of junctions attached to more than one bar (one node for each bar), which are constrained to move jointly in space [79].

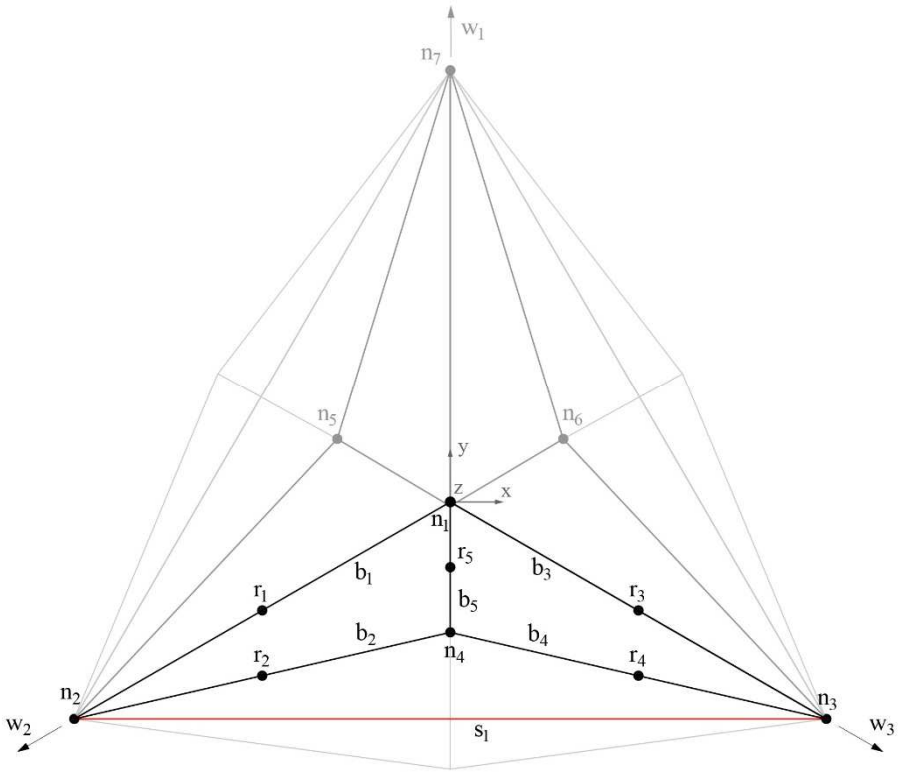

Figure 3.3: Schematic view of the WTABS tensegrity sunscreen model. The red colored members are cables; the black thick lines are bars. For graphic reasons, only one third of the basic module was highlighted, the remaining part is grayscale.

Let $\mathbf{n}_i \in R^3$ denote the generic node in the three-dimensional Euclidean space ($i \in [1,\ldots, n_n]$). We describe the positions of all the nodes through the following node matrix

$$\mathbf{N} = [\mathbf{n}_1 \ \mathbf{n}_2 \ldots \mathbf{n}_i \ldots \ \mathbf{n}_{n_n}] \in R^{3\times n_n} \tag{3.1}$$

The external force vector acting on the generic node is described by the vector $\mathbf{w}_i \in R^3$, while the overall loading condition applied to the structure is described by the following load matrix

$$\mathbf{W} = [\mathbf{w}_1 \ \mathbf{w}_2 \ldots \mathbf{w}_i \ldots \ \mathbf{w}_{n_n}] \in R^{3\times n_n} \tag{3.2}$$

We let $\mathbf{b}_k$, $\mathbf{s}_k$, $\mathbf{r}_k$ respectively denote the vector joining the end nodes of the generic bar, the vector joining the end nodes of the generic string and the position vector of the center of mass of the generic bar. The following matrices group all such vectors

$$\mathbf{B} = [\mathbf{b}_1 \ \mathbf{b}_2 \dots \mathbf{b}_k \dots \ \mathbf{b}_{n_b}] \in R^{3\times n_b} \tag{3.3}$$

$$\mathbf{S} = [\mathbf{s}_1 \ \mathbf{s}_2 \dots \mathbf{s}_k \dots \ \mathbf{s}_{n_s}] \in R^{3\times n_s} \tag{3.4}$$

$$\mathbf{R} = [\mathbf{r}_1 \ \mathbf{r}_2 \dots \mathbf{r}_k \dots \ \mathbf{r}_{n_n}] \in R^{3\times n_b} \tag{3.5}$$

Upon introducing the connectivity matrices of bars ($\mathbf{C_B} \in R^{n_b\times n_n}$), cables ($\mathbf{C_S} \in R^{n_s\times n_n}$) and centers of mass ($\mathbf{C_R} \in R^{n_b\times n_n}$), one easily obtains

$$\mathbf{B} = \mathbf{N}\mathbf{C}_\mathbf{B}^\mathbf{T}, \tag{3.6}$$

$$\mathbf{S} = \mathbf{N}\mathbf{C}_\mathbf{S}^\mathbf{T}, \tag{3.7}$$

$$\mathbf{R} = \mathbf{N}\mathbf{C}_\mathbf{R}^\mathbf{T} \tag{3.8}$$

It is useful to observe that the generic element C_{Bij} (or $\underline{C}_{Sij}$) is equal to -1 if $\mathbf{b}_i$ (or $\mathbf{s}_i$) is directed away from node *j*; 1 if such a vector is directed towards such a node, and 0 if $\mathbf{b}_i$ (or $\mathbf{s}_i$) does not touch node *j*. According to the classification introduced in [21], a tensegrity system is said of class *m*, if the maximum number of bars concurring in each node is equal to *m*. It is an easy task to verify that the WTABS module in Fig. 2(b) is a tensegrity system of class 6.

We now introduce the force density (member force divided by length) of the k^{th} cable as it follows

$$\gamma_k = \left[0, k_k\left(1 - \frac{L_k}{s_k}\right)\right] + \gamma_{ck} \tag{3.9}$$

Here, k_k is the axial stiffness coefficient of the current string, L_k is its rest length, s_k is the current length, and γ_{ck} is the force density produced by damping effects. The latter is computed as [79],[80]

$$\begin{aligned} \gamma_{ck} &= c_k \dot{s}_k / s_k, \quad if: \ s_k \geq L_k, \\ \gamma_{ck} &= 0, \qquad\quad if: \ s_k < L_k. \end{aligned} \tag{3.10}$$

Under the above settings, we can write the equations of motion of the tensegrity system under examination as follows [79]

$$\ddot{\mathbf{N}}\mathbf{M} + \mathbf{N}\mathbf{K} = \mathbf{W} \tag{3.11}$$

where

$$\mathbf{M} = \mathbf{C_B^T}\hat{\mathbf{m}}\mathbf{C_B}\frac{\mathbf{1}}{\mathbf{12}} + \mathbf{C_R^T}\hat{\mathbf{m}}\mathbf{C_R} \in R^{n_n \times n_n} \tag{3.12}$$

$$\mathbf{K} = \mathbf{C_S^T}\boldsymbol{\gamma}\mathbf{C_S} - \mathbf{C_B^T}\hat{\boldsymbol{\lambda}}\mathbf{C_B} \in R^{n_n \times n_n} \tag{3.13}$$

Here, $\hat{\lambda}$ is the force density vector of the bars defined by the following equation (Lagrange multiplier of the bar rigidity constraint [79],[80])

$$-\hat{\lambda} = \lfloor \dot{\mathbf{B}}^T \dot{\mathbf{B}} \rfloor \hat{m}\hat{l}^{-2}\frac{1}{12} + \lfloor \mathbf{B}^T(\mathbf{W} - \mathbf{S}\hat{\gamma}\mathbf{C_S})\mathbf{C_B^T} \rfloor \hat{l}^{-2}\frac{1}{2} \in R^{n_b \times n_b} \tag{3.14}$$

where $\hat{l}^{-2} \in R^{n_b \times n_b}$ is a diagonal matrix with entries $\hat{l}_k^{-2} = \|\mathbf{b}_k\|^{-2}$, and the symbol $\lfloor \cdot \rfloor$ denotes the diagonal matrix that collects the diagonal entries of matrix $[\cdot]$. It should be noted that the stiffness matrix **K** appearing in Eqn. (11) is not constant, being a function $\mathbf{K} = \mathbf{K}(t, \mathbf{N}, \dot{\mathbf{N}}, \hat{\gamma})$ of time and the mechanical variables **N**, $\dot{\mathbf{N}}$, $\hat{\gamma}$.

We employ the fourth-order Runge-Kutta algorithm described in [79],[80] to integrate the equations of motion (11) from a given initial time t_0 to a final time t_f,, using a small enough integration step dt.

Let assume an initial time t_0 and some initial condition $\mathbf{N_0}$ (initial configuration) and $\dot{\mathbf{N}}$ (initial velocity). The vector of positions, velocities and accelerations of each node are given by:

$$\begin{aligned}
\mathbf{n} &= \left[\mathbf{n}_1^{\mathbf{T}}\ \mathbf{n}_2^{\mathbf{T}}\ \ldots\ \mathbf{n}_i^{\mathbf{T}}\ \ldots\ \mathbf{n}_{n_n}^{\mathbf{T}}\right] \in \square^{3\times n_n} \\
\square\mathbf{n} &= \left[\square\mathbf{n}_1^{\mathbf{T}}\ \square\mathbf{n}_2^{\mathbf{T}}\ \ldots\ \square\mathbf{n}_i^{\mathbf{T}}\ \ldots\ \square\mathbf{n}_{n_n}^{\mathbf{T}}\right] \in \square^{3\times n_n} \\
\square\mathbf{n} &= \left[\square\mathbf{n}_1^{\mathbf{T}}\ \square\mathbf{n}_2^{\mathbf{T}}\ \ldots\ \square\mathbf{n}_i^{\mathbf{T}}\ \ldots\ \square\mathbf{n}_{n_n}^{\mathbf{T}}\right] \in \square^{3\times n_n}
\end{aligned} \tag{12}$$

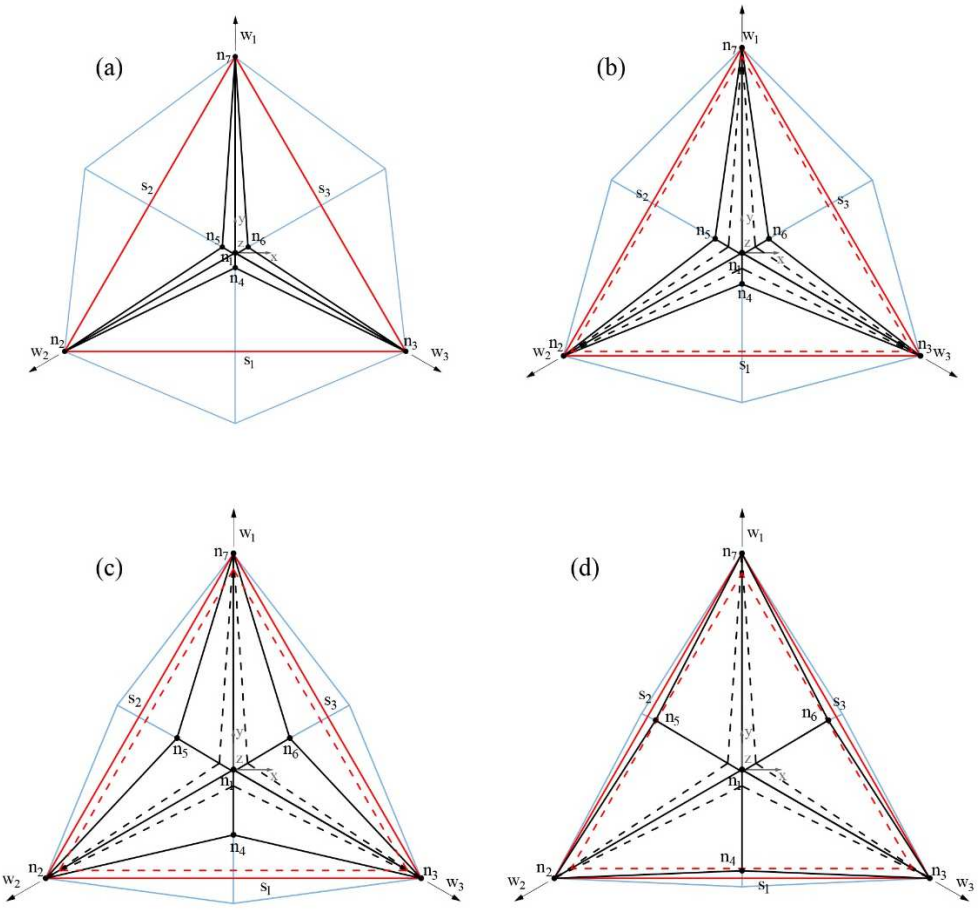

Figure 3.4: Top views of different frames of the WTABS tensegrity system actuation motion: (a) fully opened screen; (b) partially opened screen; (c) partially closed screen; (d) fully closed configuration.

Numerical results of the tensegrity shading system illustrated this chapter and dynamic simulations will be discussed in the chapter 3.2.

3.1.3 Modelling of the wind forces

Wind is a natural phenomenon that consists of the movement of air masses due to the pressure difference between two points of the atmosphere. The instantaneous wind vector speed **V** can be represented by the composition of the average speed $\mathbf{V}_m$

over an interval of 10 minutes, and the turbulence term **V**', which accounts for high frequency fluctuations [51]

$$\mathbf{V}(P,t) = \mathbf{V}_m(P) + \mathbf{V}'(P,t) \tag{3.15}$$

$$\mathbf{V}_m(P) = \boldsymbol{k}\, v_m(y) \tag{3.16}$$

$$\mathbf{V}'(P,t) = \mathbf{i}\, v'_1(P,t) + \mathbf{j}\, v'_2(P,t) + \mathbf{k}\, v'_3(P,t) \tag{3.17}$$

In the above equations above, P is any point of the space, t is the time, **i**, **j**, **k** are the unit vectors along the Cartesian axes x, y, z, such that z is perpendicular to the plane of the building façade; v_m is the average speed longitudinal at height y and v'_1, v'_2, v'_3 are the lateral (x), vertical (y) and longitudinal (z) components of turbulence.

The following analysis considers only turbulent fluctuations v'_3 and assume that such fluctuations are representable as a single stationary Gaussian random process with zero mean, which depends only on the height and time, that is $v'_3(P,t)=v'(y,t)$. Such a random variable is described by the following spectral density [51]

$$S_L(y,n) = \frac{6.8\, f_L(y,n)}{(1+10.2\, f_L(y,n))^{5/3}} \tag{3.18}$$

where $f_L(y,n)$ is a dimensionless frequency

$$f_L(y,n) = \frac{nL(y)}{v_m(y)} \tag{3.19}$$

$L(y)$ being the turbulence scale, and n the natural frequency. By choosing a frequency step Δn=0.05 Hz, and a set of 100 frequencies $n_k=(k\text{-}1/2)\,\Delta n$, we obtain [73]

$$v'(y,t) = \sum_{k=1}^{N} \sqrt{2\, S_L(y,n_k)\Delta n}\, \cos\left(2\pi n_k t + \varphi_k\right) \tag{3.20}$$

φ_k denoting randomly generated phase angles (in radians) over 0-2π. Finally, we cast the peak value of the wind kinetic pressure (in m/s) into the following form

$$q_p(y,t) = \frac{1}{2}\rho\left(v_m(y) + v'(y,t)\right)^2 \tag{3.21}$$

ρ=1.25 kg m^{-3} being the density of air.

The simulations presented in Sect. 3.3 employ numerical data corresponding to the height and the environmental conditions of the Al Bahar Towers. By setting y*=120 m in a coastal area exposed to wind, we obtain the turbulence scale $L(y^*)$=40.1589

m [51]. We consider the average velocity $v_m(y^*)$=73.4 m s^{-1}, which corresponds to the wind pressure of 3.5 kPa measured through tunnel tests on full-scale screen prototypes of the towers [38].

3.2 Numerical results of the WTABS model

We deal in the present chapter with numerical simulations of the dynamics of a WTABS module under the actuation motion (Sect. 3.3.2) and wind-induced vibrations (Sect. 4.3). Our simulations consider a damping factor of 5%, a time step of 0.025 s, and the material properties that are illustrated in the following section.

3.1.2 Material properties and effective masses

The bars of the WTABS module employ the 6082-T5 Aluminum alloy, as in the TABS design presented in [36]. The strings make use of a wire rope featuring a nylon core cable with 8.9 mm diameter, which is helically wound with a bundle of piezoelectric coaxial cables [78]. The latter are obtained by covering lightweight conductive wires with PVDF films. The PVDF films are shrouded in a copper braid and cover central stretchable wires with 2.67 mm diameter. Such a composite structure is covered with a plastic coating for protection. A total of 42 piezoelectric cables is used to form the composite wire rope. The piezo cables are organized in 6 strands twisted around the nylon core, each of which shows 7 piezo cables, as shown in Fig. 3.5. Using the Hruska's equation for the elastic response of a wire rope [81], and a 56 degree lay angle for the PVDF cables and the strands forming the rope, we predict an overall effective stiffness of the piezo-composite wire rope equal to 306.31 kN.

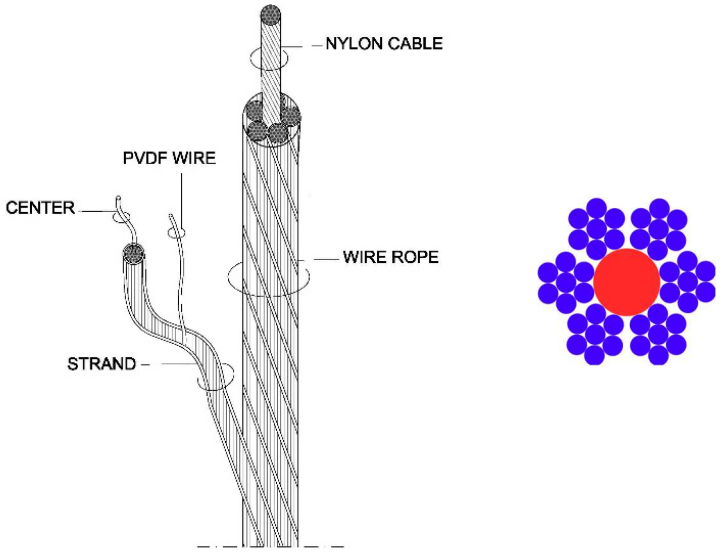

(a) (b)

Figure 3.5: (a) Assembly of the composite wire rope used for the strings of the WTABS module. (b) Cross-section of the wire showing the nylon core (red) and the outer piezoelectric cables (blue).

The mechanical model introduced in the present work makes use of effective (equivalent) masses of the bars forming the WTABS module, which account for the actual masses of the bars, and a flat-rate calculation of the masses of nodes and the secondary structural elements (infill panels, made of PTFE coated fiber glass fabrics with 1.5 kg m^{-2} mass density per unit area, guiding rails, etc.). We compute the effective masses of the bars forming the outer triangles (see Fig. 3.2(a)) by doubling the masses of the 6082-T5 Aluminum bars, whose geometric and mechanical properties are listed in Table 3.1. We instead identify the effective masses of the 36 struts forming the 6 D-bar units placed behind the infill panels (see Fig. 3.2(c)) with the actual masses, since such bars are not connected to significant secondary structural elements. The effective masses given to all the bars of the WTABS module are listed in Table 3.2. The geometrical and mechanical properties of the strings are given in Table 3.3. The masses of the such elements are lumped at the nodes.

Table 3.1: Geometric and mechanical data of 6082-T5 Aluminum bars. The area of the cross sections is computed as A0=2 t (w+h-2 t).

Width	Height	Thickness	Material	Young modulus	Density
w	h	t		E	ρ
(mm)	(mm)	(mm)		(GPa)	(kg m^{-3})
150	70	5	6082-T5	72	2.70×10^{3}

Table 3.2: Effective masses of the bars.

# Element	Length	Infill panel	Effective mass
	(m)	(kg)	(kg)
3	1.3135	1.4941	16.3888
3	2.6269	1.4941	31.2836
6	2.2750	0.7470	26.5455
18	2.2755	-	12.9020
18	1.5966	-	9.0526

Table 3.3: Geometric and mechanical properties of the strings.

Diameter d (mm)	Material	Young modulus E_s (GPa)
9	Nylon core	3.9
2.67	Piezo cable	2.7 (PVDF film)

3.2.2 Simulation of the actuation motion

The opening and closure of the external macro-triangle forming the WTABS module is activated by a force applied to a vertex (actuated node) by the linear actuator Rolaram® R2501190 [36],[37]. The actuation motion deploys the screen from the open (folded) to the closed configuration over a time window of a 40 s. The closed configuration is almost (but not completely) flat, in order to avoid the penetration of the bars forming the macro-triangles [36].

We simulate the actuation motion by applying the above loading program to the numerical model presented in Sect. 3. The total simulation time is 80 s, since we hold the push force on the actuated node constant for 40 s, after the closure of the screen. At the initial time t=0 the force on the actuated node has the value F_{min}=72.690 kN,

which is necessary to apply the initial state of folding to the module [36]. At t=40 s, the actuation force reaches its maximum value, which is equal to F_{max}=276.221 kN.

Fig. 3.6 and Fig. 3.7 illustrate three deformed configurations obtained through the numerical simulation of the actuation motion of the WTABS module, namely the initial state, an intermediate unfolded configuration reached at t = 25 s, and the deployed configuration occupied at t = 50 s (see the Appendix for an animation of the actuation motion). We assume that the actuated node is kept locked once the closed configuration has been reached. Fig. 3.6 also illustrates the time-history of the of the z-coordinate of the central node of the module during the actuation motion.

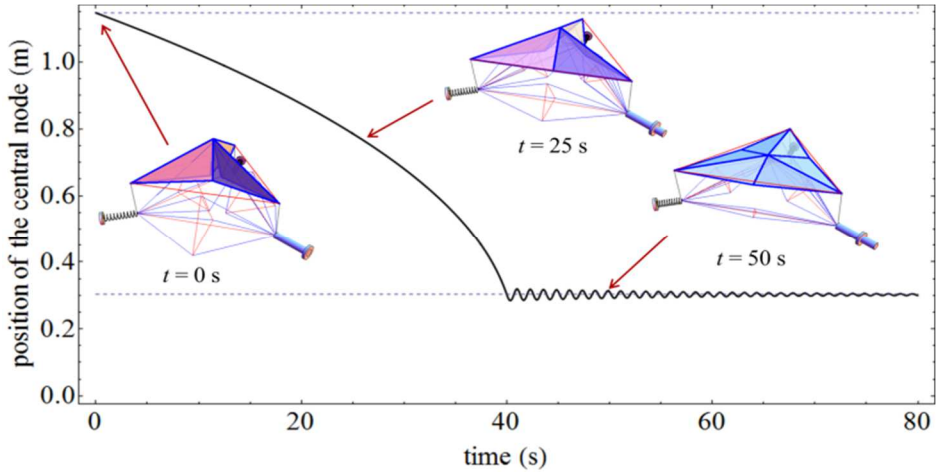

Figure 3.6: Height of the central node vs time computed through the simulation of the actuation motion of the WTABS module.

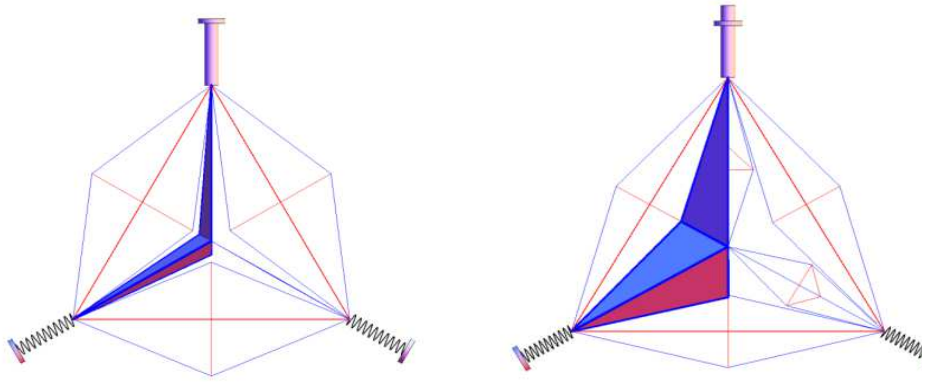

(a) (b)

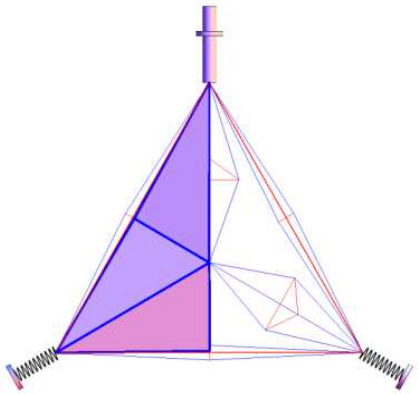

(c)

Figure 3.7: Details of selected configurations of the actuation motion of the WTABS module: open configuration at t = 0 s (a), partially closed configuration at t = 25 s (b), and closed configuration at t = 50 s (c). The boundary springs and the actuator ram are idealized and not reported in scale. (see also the animation provided as supplementary material).

3.3 Mechanical energy harvesting

3.3.1 Simulation of the wind dynamics

The simulation of the wind dynamics of the WTABS module makes use of the modelling of the wind forces described in Sect. 3.2. Such forces are assumed to act on the closed configuration of the screen depicted in Fig. 3.7(c). We prescribe zero initial nodal velocities on such a configuration, since we assume that the actuator is locked under the action of wind forces. The total simulation time is set to 250 s. Fig. 3.8 illustrates the snapshot at t=50 s extracted from the simulation of the wind dynamics of the WTABS module (see the Appendix for an animation of such a simulation). Fig. 3.9 instead illustrates the time history of the z-coordinate of the central node of the module under the action of the wind forces.

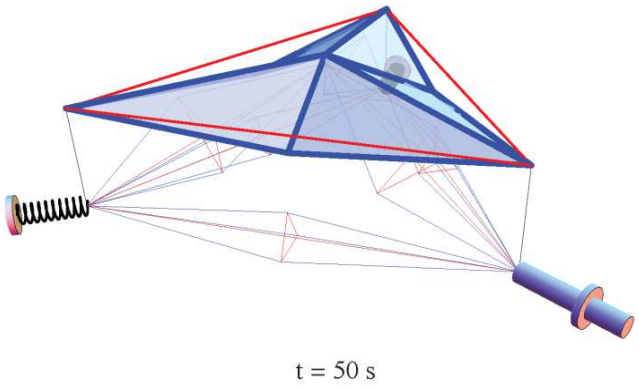

Figure 3.8: Snapshots at t=50 s from the simulation of wind dynamics of the WTABS module. The boundary springs and the actuator ram are idealized and not reported in scale. (see also the animation provided as supplementary material).

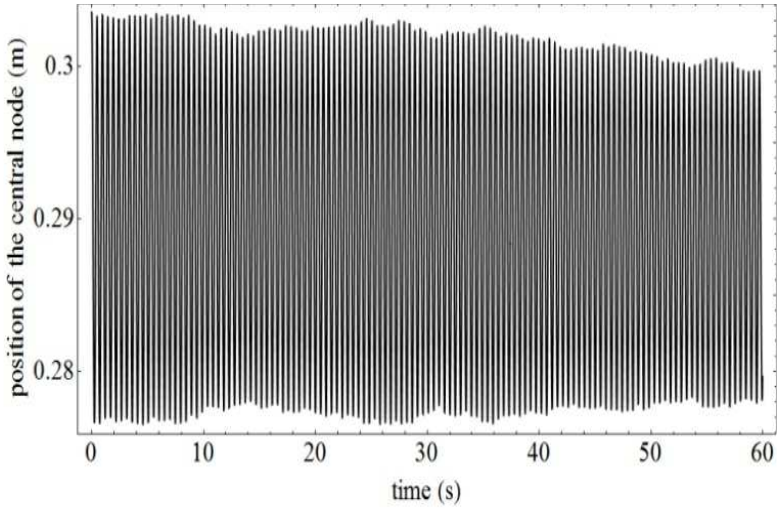

Figure 3.9: Time history of the z-coordinate of the central node of the WTABS module along the direction normal to the building façade, during the first 60 s of the simulation.

3.3.2 Wind energy harvesting sensors and actuators

The PVDF-coated piezoelectric cables composing the wire ropes of the WTABS module (Fig. 3) exhibit the mechanical properties listed in Table 3.4 (parameters imported from Refs. [78],[82],[83]). The elastic energy W_M stored into the

piezoelectric cables is converted into electric energy W_E through the electromechanical effect described by the following equation (see [84], p. 21)

$$W_E = k_{33}^2 W_M \tag{3.22}$$

where k_{33} is the electromechanical coupling coefficient along the longitudinal axis of the piezoelectric cables.

We compute W_M by making use of the strain history recorded in the strings during the simulations of the actuation motion and the wind dynamics illustrated in Sect. 4, obtaining

$$W_M = \frac{1}{2\,T} \sum_{s=1}^{n_s} \left(E_f A_f L_{is} \int_0^T \varepsilon_s(t)^2 dt \right) \tag{3.23}$$

where T is the total time of simulation, L_{is} is the initial length of the s^{th} string, n_s is the number of strings, and A_f is the area of the PVDF film.

Table 3.4. Properties of the employed piezo cable.

Material	Young's modulus	Ultimate stress	Ultimate strain	Coupling coefficient
	Ef	σf	εf	k33
	(GPa)	(MPa)	(%)	(-)
PVDF	2.7	350	16.9	0.15

With reference to the actuation motion analyzed in Sect. 4.2, Eqns. (22) -(23) allow us to predict the following overall values of the mechanical energy stored in the strings (W_M^{act}), and the electric energy produced through piezoelectric effect (W_E^{act})

$$W_M^{act} = 14082.1 \text{ kJ} = 3911.7 \text{ Wh}, \tag{3.24}$$

$$W_E^{act} = 321.3 \text{ kJ} = 89.2 \text{ Wh}. \tag{3.25}$$

A similar procedure leads us to predict the mechanical energy stored in the strings (W_M^{wind}) and the electric energy produced through piezoelectric effect (W_E^{wind}), in correspondence with the wind motion that has been studied in Sect. 4.3

$$W_M^{wind} = 25.548 \times 10^{-2} \text{ kJ} = 7.095 \times 10^{-2} \text{ Wh}, \tag{3.26}$$

$$W_E^{wind} = 5.749 \times 10^{-4} \text{ kJ} = 1.5968 \times 10^{-4} \text{ Wh}. \tag{3.27}$$

It is worth comparing the above energies with those that can be produced by photovoltaic panels and wind turbines available in the market. With reference to average values of the energies that can be produced over a day, Table 3.5 compares the electric energies per unit area produced by a WTABS module with the analogous energies that can be produced by photovoltaic (PV) panels in the area of Abu Dhabi (estimated through the PVWatts® calculator [89]) and by the microeolic wind turbines studied in [7] (most-effective rooftop setup). One observes that the energy that can be harvested per unit surface during the opening and closure of the WTABS is equal to about 3% and 1% of the energies that can be daily produced by PV panels and wind turbines, respectively. It is worth noting that the sunscreens of the Al Bahar towers include more than 1000 modules, each of which has a surface area of 8.75 m^2 [37],[38]. The overall electric energy that can be daily produced by the WTABS actuation is therefore considerable, being approximately equal to that produced by 233 PV panels and 87 microelolic rooftop turbines with 1 m^2 surface area.

Table 3.5: Comparison of the electrical energies per unit surface that can be daily produced by different energy harvesting systems.

WTABS actuation	20 Wh m^{-2}
WTABS wind	0.263 mWh m^{-2}
PV panels	750 Wh m^{-2}
Wind turbines	2000 Wh m^{-2}

The results in Table 3.5 also show that one WTABS module is able to produce about 2.3 milliwatt hour under the action of wind forces, which is sufficient to power, e.g., microelectronic devices, WiFi repeaters, cellular phones, and/or LED lighting systems [85].

Part IV. Concluding remarks and future work

4.1 Discussion and conclusion

4.1.1 Discussion and conclusion

Nowdays technological development of active solar façades is strictly tied to the production of new technologies that permit the realization of lightweight building envelopes featuring sufficiently high stiffness and stability. The lightness is a fundamental prerequisite to guarantee easy deployability of the active modules of a solar façade, in order to reduce overall costs, and to favor easy installation and transportation of the structure.

We have shown in this thesis that tensegrity concepts can be profitably employed to design dynamic sun screens that exhibit a morphing-type response, with limited use of materials and very low energy consumption. A tensegrity design of dynamic sun screens that replicate the origami screens of the Al Bahar towers in Abu Dhabi has been presented, by deriving the exact kinematics of the modules forming such screens, conducting the stress-analysis of the investigated structures under the actuation motion and wind loading, and estimating their weight and activation energy.

We have shown that the tensegrity design formulated in the present work leads us to approximately obtain a 50% weight reduction over the ABS design reported in Armstrong et al. (2013) [37]. Such a result leads to marked improvements of the system performance in terms of the environmental impact of the construction process, due to a significant reduction of construction materials (Section 2.4), which is known to greatly influence the building's carbon emissions over its lifetime (Construction, 2018), while keeping the U-value (the insulation characteristics) and the G-value (the shading coefficient) of the façade unchanged with respect to the ABS design (as a consequence of the use of identical geometry and materials of the infill panels).

The structures presented in this thesis allow us to create "tensegrity skins" of energy efficient buildings, which can serve as lightweight shading envelopes and are, at the same time, able to harvest solar and wind energies. Since the units of such skins are controlled by stretching or relaxing selected cables, suitably designed tensegrity

systems can indeed be used not only as shading barriers, but also as actuators orienting solar panels toward the sun, and/or as novel micro-eolic power generators converting the wind-excited strain energy of the cables into electrical power [21].

Tensegrity structures have the special ability to act as lightweight deployable systems with "morphing" abilities [29],[36],[86]-[88]. Making use of tensegrity concepts, we have generalized the design of the TABS sunscreens, in order to endow such structures with mechanical energy harvesting ability. We have proposed novel sunscreens, named WTABS, whose unit cell is obtained by complementing the TABS module with a set of D-bar units placed in the space running between the screens and the building façade. We have simulated the dynamics of the WTABS module in correspondence with the actuation motion and wind forces, making use of a mixed, rigid body (bars) – elastic springs (strings) mechanical model.

The results presented in Section 3 have led us to predict the amount of mechanical energy that can be harvested through piezoelectric effects by the WTABS structures. It has been shown that each of the sunscreens protecting the Al Bahar towers can daily produce a quantity of electric energy equal to that produced by about 233 m^2 of PV panels and 87 m^2 of rooftop wind turbines, due do the electromechanical conversion of the energy stored in the piezoelectric cables during the actuation motion. The energy that can be harvested under the action of wind forces is markedly lower, being however sufficient to power microelectronic devices and wireless systems [85].

This PhD thesis promotes an innovative technological solution as the way forward to design higher performance building shading façades. We have investigated on the use of tensegrity systems to optimize the active shading screens of the Al Bahar Towers based on kinematics analysis of tensegrity structures. The result is a deployable tensegrity skin system, able to harvest solar energy and to react differently according to the sun's orientation, so the building's envelope is constantly evolving, reflecting the seasonal natural rhythms.

Tensegrity systems have been employed for different engineering uses and their dynamic control is performed by acting on the pretension of the cables (by controlling the elongation in a limited number of cables). The morphing capacity of such structures allows the design of active sunscreens that result in reduced frictional effects between the elements and requires limited energy consumption for their implementation.

4.1.2 Future research

Possible future applications of tensegrity dynamic structures will certainly have to be based on an approach directed towards the functionality of such systems in relation to the main characteristics that distinguish them, namely lightness, the ability to control and the high aesthetic value. In the field of research, aspects such as eco-sustainability, functionality and minimum mass must be the key concepts for the design of active solar façades of next generation smart buildings.

As regards future research lines that are worthy of further study we can focus on the possibility of using different materials as, for example, composite materials which have different parametric properties and could guarantee advantages from the point of view of mechanical response; the possibility to design different dynamic solar shading façades using topological coordinates of different architectural forms with energy optimization techniques; the potential applications of the rapid prototyping systems for the optimal design of architectural origami façades and deployable space structures responding to the external environment.

We address such generalizations and extensions of the analyzed tensegrity systems to future work, with the aim of designing solar façades featuring various geometries and deployment schemes, and understanding the versatility of the tensegrity architectures across different scales of the unit cells. Such studies will make use of fractal geometry [22], parametric design concepts [63] and advanced computational models [54].

Additional future research lines will be oriented to investigate the application of 3D- and 4D-printing technologies for the fabrication of reduced-scale mockups of active tensegrity façades [24]. We plan to tackle the technological challenge related to the application of the internal prestress by recourse to multimaterial 3D printing technologies that use materials with different thermohygroscopic properties (see e.g., the polyjet technology described in [69]).

Furthermore, future directions of the present study may be addressed to the design of dynamic deployable structures supporting hybrid double-skin façades, which couple natural or mechanical ventilation systems with adaptive shading technologies [90]. We also plan to investigate the use of different piezoelectric materials, such as piezo ceramics, composites, polymers and monocrystals [77],[78], in order to improve and to optimize the energy harvesting capacity of the WTABS shading system presented in the second part of the thesis.

BIBLIOGRAPHY

[1] Directive (UE) 2018/844. European Parliament and of the Council of 30 May 2018 on Energy Efficiency, Amending Directives 2012/27/UE and 2010/31/EU.

[2] Quesada, G., Rousse, D., Dutil, Y., Badache, M., and Hallé, S. (2012a). A comprehensive review of solar façades. Opaque solar façades Renew. Sust. Energ. Rev. 16, 2820–2832. doi: 10.1093/ijlct/ctv020

[3] Quesada, G., Rousse, D., Dutil, Y., Badache, M., and Hallé, S. (2012b). A comprehensive review of solar façades. Transparent and translucent solar façades Renew. Sust. Energ. Rev. 16, 2643–2651. doi: 10.1016/j.rser.2012.01.078

[4] Schittich, C., (ed.). (2003). "Solar architecture. Strategies, visions, concepts," in Detail Series. München: Birkhäuser Architecture.

[5] Kuhn, T. E., Herkel, S., and Henning, H.-M. (2010). "Active solar façades (PV and solar thermal)," in PALENC 2010. Available online at: http://publica.fraunhofer.de/documents/N-161087.html

[6] Bai, Y., Jantunen, H., and Juuti, J. (2018). Hybrid, multi-source, and integrated energy harvesters. Front. Mater. 5:65. doi: 10.3389/fmats.2018.00065

[7] Balduzzi, F., Bianchini, A., and Ferrari, L. (2012). Microeolic turbines in the built environment: influence of the installation site on the potential energy yield. Renew. Energ. 45, 163–174. doi: 10.1016/j.renene.2012.02.022

[8] Herzog, T., Flagge, I., Herzog-Loibl, V., Meseure, A., Architekturmuseum, D.: Thomas Herzog: Architektur + Technologie. Architecture Series. Prestel (2001).

[9] Directive 2010/31/EU of the European Parliament and of the Council of 19 May 2010 on the energy performance of buildings.

[10] Pérez-Lombard, L., Ortiz, J., Pout, C.: A review on buildings energy consumption information. Energy and Buildings 40(3), 394–398 (2008). DOI 10.1016/j.enbuild.2007. 03.007.

[11] Alotaibi F (2015) The Role of Kinetic Envelopes to Improve Energy Performance in Buildings. J. Archit. Eng. Tech. 4: 149. doi:10.4172/2168-9717.1000149.

[12] European Commission, HORIZON 2020 Work Programme 2014-2015, PART 5.ii, p. 98, 2014.

[13] Baldinelli G., Double skin façades for warm climate regions: Analysis of a solution with an integrated movable shading system. Build and Environ 2009; 44: 1107-1118.

[14] Mainini AG, Poli T, Zinzi M, Speroni A, Spectral light transmission measure of metal screens for glass façades and assessment of their shading potential, SHC 2013, In: Proceedings of International Conference on Solar Heating and Cooling for Buildings and Industry. Freiburg, September, 2013.

[15] Bianco JM, Buruaga A, Roji E, Cuadado J, Pelaz B. Energy assessment and optimization of perforated metal sheet double skin façades through Design Builder; A case study in Spain. Energ Buildings 2016; 111: 326-336.

[16] Mammoli A, Vorobieff P, Barsun H, Burnett R, Fisher D. Energetic, economic and environmental performance of a solar-thermal- assisted HVAC system. Energ Buildings 2010; 42: 1524-1535.

[17] Green Building Council Italia, U.S. Green Building Council. Green Building Nuove Costruzioni & Ristrutturazioni - ristampa 2011. Rovereto: Green Building Council, 2010. (in Italian)

[18] Asdrubali F, Baldinelli G, Bianchi F, Sambuco S. A comparison between environmental sustainability rating systems LEED and ITACA for residential buildings. Build and Environ 2015; 86: 98-108.

[19] Directive 2002/91/EC of the European Parliament and of the Council of 16 December 2002 on the energy performance of buildings.

[20] Magrini A, D'Ambrosio Alfano FR, Magnani L, Pernetti R. Various approaches to the evaluation of the energy performance of buildings in Italy-some results of calculation procedures application on residential buildings. In: Proceedings of CESB 2010 Prague - Central Europe towards Sustainable Building 'From Theory to Practice'. Prague; June-July 2010. Code 105800. pp. 1-8.

[21] Skelton RE, de Oliveira MC. Tensegrity Systems. New York: Springer Science+Business Media, 2009.

[22] Skelton RE, Fraternali F, Carpentieri G, Micheletti A. Minimum mass design of tensegrity bridges with parametric architecture and multiscale complexity. Mech Res Commun 2014; 58: 124-132.

[23] Carpentieri G, Skelton RE, Fraternali F. Minimum mass and optimal complexity of planar tensegrity bridges. International Journal Space Structure 2015; 30(3–4):221–244.

[24] Amendola A, Carpentieri G, De Oliveira M, Skelton, R.E., Fraternali, F., Experimental investigation of the softening-stiffening response of tensegrity prisms under compressive loading. Compos Struct 2014:117:234-243.

[25] Fraternali F, Carpentieri G, Amendola A. On the mechanical modeling of the extreme softening/stiffening response of axially loaded tensegrity prisms. J Mech Phys Solids 2014; 74:136-157.

[26] Fraternali F, Senatore L, Daraio C. Solitary waves on tensegrity lattices. J Mech Phys Solids 2012; 60:1137-1144.

[27] Fraternali F, Carpentieri G, Amendola A, Skelton RE, Nesterenko VF. Multiscale tunability of solitary wave dynamics in tensegrity metamaterials. Appl Phys Lett 2014:105:201903

[28] Fraternali F, De Chiara E, Skelton RE. On the use of morphing and wind stable tensegrity structures for shading façades of smart buildings. Smart Mater Struct 2015; 24, 105032 (10pp).

[29] Cimmino, M. C., Miranda, R., Sicignano, E., Ferreira, A. J. M., Skelton, R. E., and Fraternali, F. (2017). Composite solar façades and wind generators with tensegrity architecture. Compos. B Eng. 115, 275–281. doi: 10.1016/j.compositesb.2016.09.077.

[30] Dinh Quy V, Van Sy N, Tan Hung D, Quoc Huy V. Wind tunnel and initial field tests of a micro generator powered by fluid-induced flutter. Energy for Sustainable Development 2016; 33:75-83.

[31] Arroyo E, Foong S, Wood KL. Modeling and experimental characterization of a fluttering windbelt for energy harvesting. Journal of Physics: Conference Series 2014; 557 (1), art. no. 012089

[32] Kneepens, Steven & Knol, Alois & Zvironaite, Kotryna (2015), KINETICA: A Playful Way Through The World Of Moving Façades. Amsterdam, The Netherlands, Architectural Engineering and Technology, 35 p.

[33] Aelenei, Laura & Aelenei, Daniel & Romano, Rosa & Mazzucchelli, Enrico & Marcin, Brzezicki & Rico-Martinez, Jose Miguel. (2018). Case Studies - Adaptive Façade Network.

[34] Herzog, T., Ed. - SOKA-BAU: Utility, Sustainability, Efficiency. Munich: Prestel, 2006.

[35] Herzog, T. - Extension to the head office of SOKA-BAU, the pensions and benefits fund of the German building industry, in Wiesbaden a new multi-use building with offices, restaurant, conference, computer center - 1994-2004. In Proceedings of PLEA 2006 - The 23rd Conference on Passive and Low Energy Architecture, Geneva, Switzerland, 6-8 September, 2006.

[36] Babilio, E., Miranda, R., Fraternali, F.: On the kinematics and actuation of dynamic sunscreens with tensegrity architecture. Frontiers in Materials 6 (2019). DOI 10.3389/ fmats.2019.00007.

[37] Armstrong, A., Buffoni, G., Eames, D., James, R., Lang, L., Lyle, J., Xuereb, K.: The Al Bahar towers: multidisciplinary design for middle east high-rise, abu dhabi, united arab emirates. The Arup Journal 2, 60–73 (2013).

[38] Karanouh, A., Kerber, E.: Innovations in dynamic architecture. Journal of Façade Design and Engineering 3(2), 185–221 (2015). DOI 10.3233/FDE-150040.

[39] Snelson K., Kenneth Snelson, New York, U.S.A., 2004.

[40] Fuller R. B./Applewhite E. J., Synergetics: Explorations in the Geometry of Thinking, New York, MacMillan Publishing Co. Inc., 1975.

[41] Wagner R., The virtual world of "Tensional Integrity", Munich, Germany, University of applied science.

[42] Motro R., Tensegrity – Structural Systems for the Future, London, UK, Kogan Page Science, 2003.

[43] Micheletti A., Torri Tensintegre, tesi di dottorato, Roma, Dipartimento di Ingegneria Civile, Università di "Tor Vergata", 2003.

[44] Gómez Jáuregui V., Tensegrity Structures and their Application to Architecture, tesi di dottorato, Queen's University, School of Architecture, Belfast, Northern Ireland, 2004.

[45] Al-Kodmany, K. (2016). Sustainable tall buildings: cases from the global south. Arch. Int. J. Archit. Res. 10, 52–66. doi: 10.26687/archnet-ijar.v10i2.1054

[46] Amendola, A., Nava, E. H., Goodall, R., Todd, I., Skelton, R. E., and Fraternali, F. (2015). On the additive manufacturing, post-tensioning and testing of bi-material tensegrity structures. Compos. Struct. 131, 66–71. doi: 10.1016/j.compstruct.2015.04.038

[47] Attia, S. (2017). Evaluation of adaptive façades: the case study of Al Bahr Towers in the UAE. Sci. Connect Shap. Qatar's Sustain. Built Environ. 2 2017:6. doi: 10.5339/connect.2017.qgbc.6

[48] Blaise, N., and Denoël, V. (2013). Principal static wind loads. J. Wind Eng. Ind. Aerodyn. 113, 29–39. doi: 10.1016/j.jweia.2012.12.009

[49] Construction (2018). Construction, Real Estate, and Carbon Emissions. Available online at: https://climatesmartbusiness.com/wp-content/uploads/2013/10/CSConstruction-Industry-Brief.pdf

[50] Directive (UE) 2018/844. European Parliament and of the Council of 30 May 2018 on Energy Efficiency, Amending Directives 2012/27/UE and 2010/31/EU.

[51] EN 1991-1-4 (2005). (English): Eurocode 1: Actions on Structures - Part 1-4: General actions - Wind Actions. (Authority: The European Union Per Regulation 305/2011, Directive 98/34/EC, Directive 2004/18/EC).

[52] Fleck, N. A., Deshpande, V. S., and Ashby, M. F. (2010). Micro-architectured materials: past, present and future. Proc. R. Soc. A 466, 2495–516. doi: 10.1098/rspa.2010.0215

[53] Hutchinson, R. G., and Fleck, N. A. (2006). The structural performance of the periodic truss. J. Mech. Phys. Solids 54, 756–782. doi: 10.1016/j.jmps.2005.10.008

[54] Infuso, A., and Paggi, M. (2015). Computational modeling of discrete mechanical systems and complex networks: where we are and where we are going. Front. Mater. 2:18. doi: 10.3389/fmats.2015.00018

[55] Kuhn, T. E., Herkel, S., and Henning, H.-M. (2010). "Active solar façades (PV and solar thermal)," in PALENC 2010. Available online at: http://publica.fraunhofer.de/documents/N-161087.html

[56] Lombard, L. P., Ortiz, J., and Pout, C. (2010). A review on buildings energy consumption information. Energ. Build. 40, 394–398. doi: 10.1016/j.enbuild.2007.03.007

[57] Mascolo, I., Amendola, A., Zuccaro, G., Feo, L., and Fraternali, F. (2018). On the geometrically nonlinear elastic response of class θ = 1 tensegrity prisms. Front. Mater. 5:16. doi: 10.3389/fmats.2018.00016

[58] Mazzolani, F. (1994). Aluminum Alloy Structures. London: CRC Press.

[59] R. Miranda, E. Babilio, N. Singh, F. Santos, F. Fraternali, Mechanics of smart origami sunscreens with mechanical energy harvesting ability, Mechanics Research Communications;

[60] Modano, M., Mascolo, I., Fraternali, F., and Bieniek, Z. (2018). Numerical and analytical approaches to the self-equilibrium problem of class θ = 1 tensegrity metamaterials. Front. Mater. 5:5. doi: 10.3389/fmats.2018.00005

[61] Naveen, J., Jawaid, M., Zainudin, E. S., Sultan, M. T. H., and Yahaya, R. B. (2018). Selection of natural fiber for hybrid kevlar/natural fiber reinforced polymer composites for personal body armor by using analytical hierarchy process. Front. Mater. 5:52. doi: 10.3389/fmats.2018.00052

[62] Nylonrope (2018). Quality Nylon Rope, Nylon Ropes and Cords. Available online at: https://www.qualitynylonrope.com/all-products/nylon/

[63] Pottman, H., Asperl, A., and Kilian, A. (2007). Architectural Geometry. Exton, PA: Bentley Institute Press.

[64] Power Jacks. (2018). Rolaram, Electric Linear Actuators. Available online at: https://www.powerjacks.com/perch/resources/brochure/pjlab-rolaram-en-01-1b.pdf

[65] Quesada, G., Rousse, D., Dutil, Y., Badache, M., and Hallé, S. (2012a). A comprehensive review of solar façades. Opaque solar façades Renew. Sust. Energ. Rev. 16, 2820–2832. doi: 10.1093/ijlct/ctv020

[66] Quesada, G., Rousse, D., Dutil, Y., Badache, M., and Hallé, S. (2012b). A comprehensive review of solar façades. Transparent and translucent solar façades Renew. Sust. Energ. Rev. 16, 2643–2651. doi: 10.1016/j.rser.2012.01.078

[67] Schittich, C., (ed.). (2003). "Solar architecture. Strategies, visions, concepts," in Detail Series. München: Birkhäuser Architecture.

[68] Soru, M. (2014). A Spatial Kinetic Structure Applied to an Active Acoustic Ceiling for a Multipurpose Theatre. MSc. thesis report, Delft University of Technology, Faculty of Civil Engineering and Geosciences, Track Structural Engineering.

[69] Stratasys (2018). PolyJet Technology. Available online at: https://www.stratasys.com/it/polyjet-technology

[70] Structurflex (2018). PTFE Fiberglass. Available online at: https://www.structurflex.com/materials/ptfe-fiberglass/

[71] D. McFarquhar. The role of the building façade - Curtain walls, in: Proceedings of the BEST3 - Building Enclosure Science & Technology Conference. ⟨www.brikbase.org/content/role-building-fa%C3%A7ade-%E2%80%93-curtain-walls⟩.

[72] C. Bedon, X. Zhang, F. Santos, D. Honfi, M. Kozłowski, M. Arrigoni, L. Figuli, D. Lange, Performance of structural glass façades under extreme loads – Design methods, existing research, current issues and trends, Constr. Build. Mater. 163 (2018) 921–937.

[73] Santos, Filipe & F. Gonc¸alves, Pedro & Cismasiu, Corneliu & Mauricio, Gamboa-Marrufo. (2014). Smart glass façade subjected to wind loadings. Structures & Buildings. 167. 10.1680/stbu.13.00011.

[74] K. Nagase, T. Yamashita, N. Kawabata, On a connectivity matrix formula for tensegrity prism plates, Mechanics Research Communications, Volume 77, 2016, Pages 29-43, doi.org/10.1016/j.mechrescom.2016.08.003.

[75] Xian Xu, Sili Li, Yaozhi Luo, Form-finding of a new kind of tensegrity tori using overlapping modules, Mechanics Research Communications, Volume 84, 2017, Pages 1-7, doi.org/10.1016/j.mechrescom.2017.05.011.

[76] Heping Liu, Jingyao Zhang, Makoto Ohsaki, 3-bar tensegrity units with non-equilateral triangle on an end plane, Mechanics Research Communications, Volume 92, 2018, Pages 124-130, doi.org/10.1016/j.mechrescom.2018.08.003.

[77] Park, Sanghoon & Kim, Yura & Jung, Hyosub & Park, Jun-Young & Lee, Naesung & Seo, Yongho. (2017). Energy harvesting efficiency of piezoelectric polymer film with graphene and metal electrodes. Scientific Reports. 7. 10.1038/s41598-017-17791-3.

[78] Matthew N. Silleto, Sang-Jae Yoon and Kazuo Arakawa, Piezoelectric cable macro-fiber composites for use in energy harvesting, Int. J. Energy Res. 2015; 39:120–127.

[79] Nagase, K., Skelton, R.E., Network and vector forms of tensegrity system dynamics, Mechanics Research Communicastions, 2014, 59, 14–25.

[80] Fabbrocino, F., Carpentieri, G.: Three-dimensional modeling of the wave dynamics of tensegrity lattices. Composite Structures 173, 9–16 (2017). DOI 10.1016/j.compstruct. 2017.03.102.

[81] Strzemiecki, J. and Hobbs, R. E. Properties of wire rope under various fatigue loadings. CESLIC Report SC6, Civil Engineering Department, Imperial College, London,1988.

[82] Holloway F.C. (1997) Material Characterization of Poly (vinylidene Fluoride): a Thin Film Piezoelectric Polymer, Montana State University- Bozeman, thesis for the degree Of Master of Science in Mechanical Engineering.

[83] Grzybek D., Piezoelectric generators: materials and structures. Pomiary Automatyka Robotyka 17, 2013. DOI: 10.14313/PAR_200/123.

[84] Reza Moheimani S.O. & Fleming A.J. (2006) Piezoelectric Transducers for Vibration Control and Damping. Advances in Industrial Control. Springer, London. DOI 10.1007/1-84628-332-9.

[85] G. De Pasquale, 11 - Energy harvesters for powering wireless systems*, Editor(s): Deepak Uttamchandani, In Woodhead Publishing Series in Electronic and Optical Materials, Handbook of Mems for Wireless and Mobile Applications, Woodhead Publishing, 2013, Pages 345-400, ISBN 9780857092717, doi.org/10.1533/9780857098610.2.345.

[86] Jianguo Cai, Xinyu Wang, Ruiguo Yang, Jian Feng, Mechanical behavior of tensegrity structures with High-mode imperfections, Mechanics Research Communications, Volume 94, 2018, Pages 58-63, doi.org/10.1016/j.mechrescom.2018.09.006.

[87] Yao Chen, Jiayi Yan, Jian Feng, Stiffness contributions of tension structures evaluated from the levels of components and symmetry subspaces, Mechanics Research Communications, 2019, 103401, doi.org/10.1016/j.mechrescom.2019.103401.

[88] Shuo Ma, Xing-Fei Yuan, Akram Samy, Shape optimization of a new tensegrity torus, Mechanics Research Communications, Volume 100, 2019, 103396, doi.org/10.1016/j.mechrescom.2019.103396.

[89] PVWatts® calculator, National Renewable Energy Laboratory, U.S. Dept. of Energy. Available at: https://pvwatts.nrel.gov/pvwatts.php. Date accessed: 22 Sept. 2019.

[90] Boake, T M, The Tectonics of the Double Skin: Green Building or Just More Hi-Tech Hi Jinx? – What are Double Skin Facades and How Do They Work?

ARCC/EAAE International Conference on Architectural Research, Montreal, May 2002 from www.architecture.uwaterloo.ca/faculty_projects/terri/pdf/tectonic.pdf 2002.

La borsa di dottorato è stata cofinanziata con risorse del
Programma Operativo Nazionale Ricerca e Innovazione 2014-2020 (CCI 2014IT16M2OP005),
Fondo Sociale Europeo, Azione I.1 "Dottorati Innovativi con caratterizzazione Industriale"